AD-A048 200 OREGON GRADUATE CENTER BEAVERTON F/G 9/2
FIELD ELECTRON AND ION SOURCE RESEARCH FOR HIGH DENSITY INFORMA--ETC(U)
APR 77 L W SWANSON F33615-76-C-1327
UNCLASSIFIED AFAL-TR-77-34 NL

1 OF 1
ADA048 200

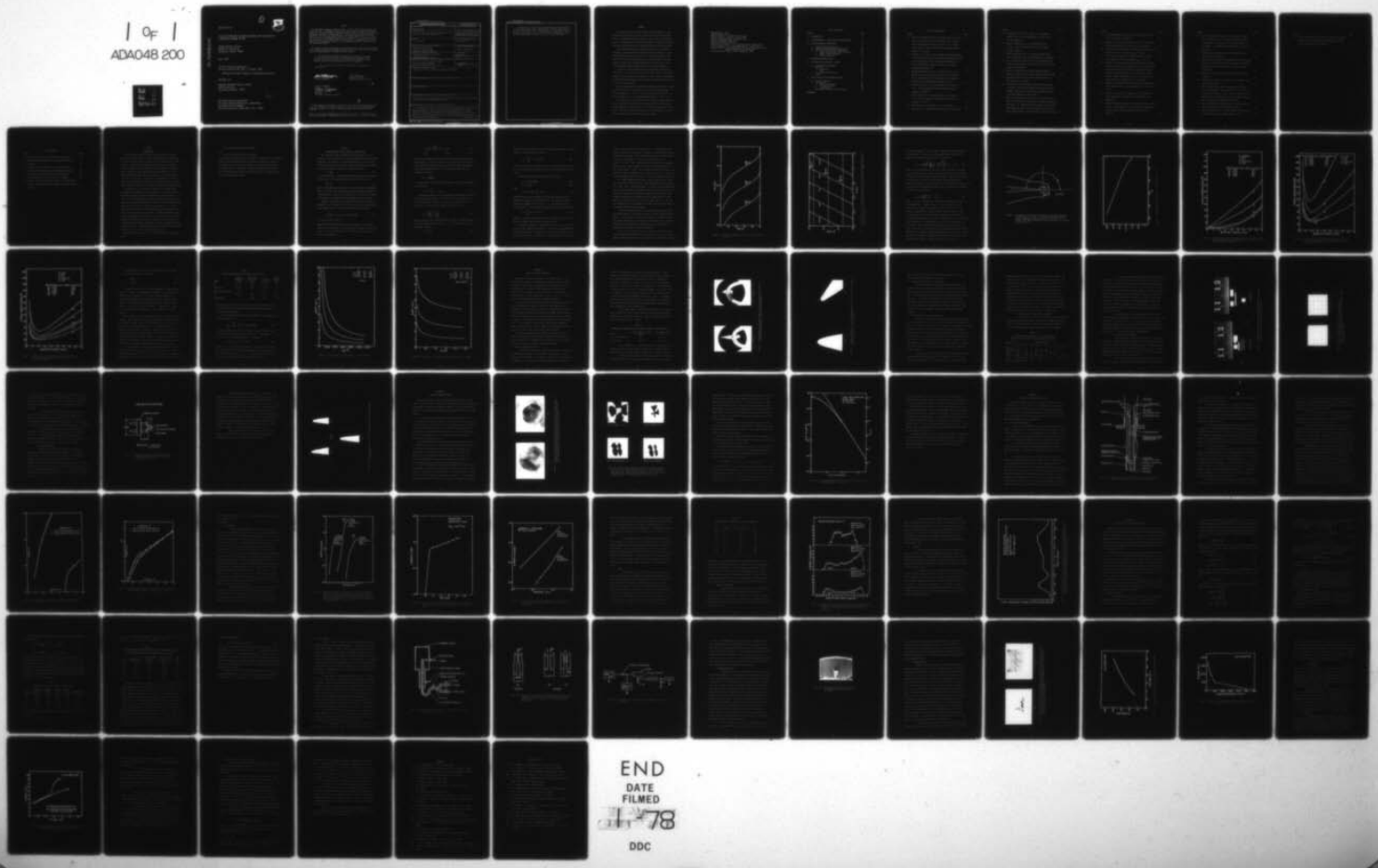

END
DATE FILMED
1-78
DDC

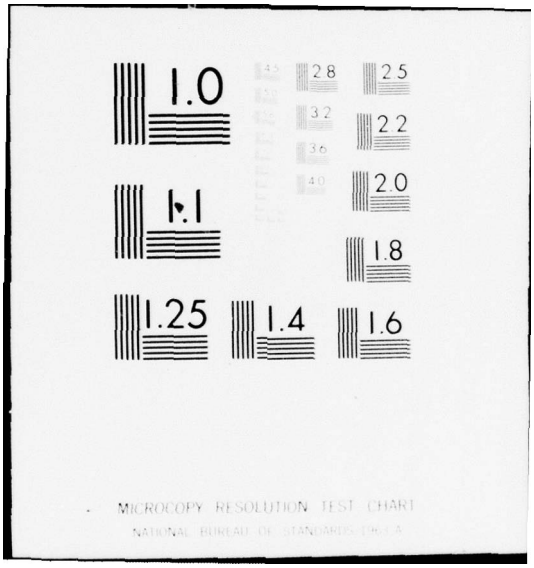
1.0
1.1
1.25
1.4
1.6
1.8
2.0
2.2
2.5
2.8
3.2
3.6
4.0
MICROCOPY RESOLUTION TEST CHART
NATIONAL BUREAU OF STANDARDS-1963-A

(1)

AFAL-TR-77-34

FIELD ELECTRON AND ION SOURCE RESEARCH FOR HIGH DENSITY INFORMATION STORAGE SYSTEM

OREGON GRADUATE CENTER
19600 N.W. WALKER RD.
BEAVERTON, OREGON 97005

APRIL 1977

INTERIM TECHNICAL REPORT NO. 1
FOR THE PERIOD 15 MAY 1976 - 15 AUGUST 1976

APPROVED FOR PUBLIC RELEASE; DISTRIBUTION UNLIMITED

PREPARED FOR

ADVANCED RESEARCH PROJECTS AGENCY
1400 WILSON BLVD.
ARLINGTON, VIRGINIA 22209

AIR FORCE AVIONICS LABORATORY
AIR FORCE WRIGHT AERONAUTICAL LABORATORIES
AIR FORCE SYSTEMS COMMAND
WRIGHT-PATTERSON AIR FORCE BASE, OHIO 45433

NOTICE

When Government drawings, specifications, or other data are used for any purpose other than in connection with a definitely related Government procurement operation, the United States Government thereby incurs no responsibility nor any obligation whatsoever; and the fact that the government may have formulated, furnished, or in any way supplied the said drawings, specifications, or other data, is not to be regarded by implication or otherwise as in any manner licensing the holder or any other person or corporation, or conveying any rights or permission to manufacture, use, or sell any patented invention that may in any way be related thereto.

This report has been reviewed by the Information Office (OI) and is releasable to the National Technical Information Service (NTIS). At NTIS, it will be available to the general public, including foreign nations.

The views and conclusions contained in this document are those of the authors and should not be interpreted as necessarily representing the official policies, either expressed or implied, of the Advanced Research Projects Agency or the U.S. Government.

This technical report has been reviewed and is approved for publication.

John M. Blasingame
John M. Blasingame
Project Engineer

Robert D. Larson
Robert D. Larson
Electronic Research Branch

FOR THE COMMANDER

William J. Edwards
WILLIAM J. EDWARDS
Director
Electronic Technology Division

"If your address has changed, if you wish to be removed from our mailing list, or if the addressee is no longer employed by your organization please notify AFAL/DHR *,W-PAFB, OH 45433 to help us maintain a current mailing list".*

Copies of this report should not be returned unless return is required by security considerations, contractual obligations, or notice on a specific document.

Unclassified

SECURITY CLASSIFICATION OF THIS PAGE *(When Data Entered)*

REPORT DOCUMENTATION PAGE		READ INSTRUCTIONS BEFORE COMPLETING FORM
1. REPORT NUMBER AFAL-TR-77-34	2. GOVT ACCESSION NO.	3. RECIPIENT'S CATALOG NUMBER
4. TITLE *(and Subtitle)* FIELD ELECTRON AND ION SOURCE RESEARCH FOR HIGH DENSITY INFORMATION STORAGE SYSTEM		5. TYPE OF REPORT & PERIOD COVERED Interim Technical Report No.1 15 May 1976 - 15 Aug. 1976
		6. PERFORMING ORG. REPORT NUMBER
7. AUTHOR*(s)* L. W. Swanson		8. CONTRACT OR GRANT NUMBER*(s)* F33615-76-C-1327
9. PERFORMING ORGANIZATION NAME AND ADDRESS Oregon Graduate Center 19600 N. W. Walker Road Beaverton, Oregon 97005		10. PROGRAM ELEMENT, PROJECT, TASK AREA & WORK UNIT NUMBERS Project 3164-01-01
11. CONTROLLING OFFICE NAME AND ADDRESS Advanced Research Projects Agency 1400 Wilson Blvd. Arlington, Virginia 22209		12. REPORT DATE April 1977 13. NUMBER OF PAGES 76
14. MONITORING AGENCY NAME & ADDRESS*(if different from Controlling Office)* Air Force Avionics Laboratory (DHR) Air Force Systems Command Wright Patterson AFB, Ohio 45433		15. SECURITY CLASS. *(of this report)* Unclassified 15a. DECLASSIFICATION/DOWNGRADING SCHEDULE
16. DISTRIBUTION STATEMENT *(of this Report)* Approved for public release; distribution unlimited		
17. DISTRIBUTION STATEMENT *(of the abstract entered in Block 20, if different from Report)*		
18. SUPPLEMENTARY NOTES		
19. KEY WORDS *(Continue on reverse side if necessary and identify by block number)* Field emission, field ion emission, field electron emission, high brightness electron source, high brightness ion source		
20. ABSTRACT *(Continue on reverse side if necessary and identify by block number)* The purpose of this research program is the development of high brightness field emission sources of both ions and electrons by use of field emission phenomena. Fabrication procedures and evaluation of emission characteristics have been examined for lanthanum hexaboride field electron emitters. Field electron emission from a liquid gallium source has also been developed and examined. Emission occurs in a pulse mode with 50 to 100 A peak currents in 10 nsec pulses. (continued)		

DD FORM 1 JAN 73 1473 EDITION OF 1 NOV 65 IS OBSOLETE

Unclassified

SECURITY CLASSIFICATION OF THIS PAGE *(When Data Entered)*

Gas phase field ion emission using hydrogen has been examined using a high pressure source configuration. Current intensities of 5×10^{-5} A Sr^{-1} $torr^{-1}$ at 77 K were measured. In addition, a preliminary investigation of ion emission from a liquid gallium source has shown that stable currents up to 150 μA can be obtained.

SUMMARY

The purpose of this research program is the development of high brightness field emission sources of both ions and electrons suitable for use in information storage systems. In particular, field electron sources of various types of materials and modes of operation along with gas phase and liquid film field ionization sources are being examined.

Fabrication procedures for producing single crystal emitters of lanthanum, cerium and samarium hexaboride have been developed. Field electron emission characteristics such as energy distribution, noise, emitter life, and I(V) characteristics are being examined. Improved methods of fabricating existing thermal-field electron sources such as the zirconium coated tungsten source are also being developed.

A new type of electron emission source employing liquid gallium formed into a cone shaped structure by an applied electric field appears capable of very intense electron emission. Thus far only a pulsed mode of emission has been observed with extraordinary high peak currents of 50 to 100 A in 10 nsec pulses.

Source configuration development and emission characteristic studies have been carried out for gas phase field ionization using hydrogen. A source brightness of $\sim 10^{7}$ A sr^{-1} cm^{-2} has been measured for H_2^+ at an emitter temperature of 77 K and hydrogen pressure of 1×10^{-2} torr.

A liquid metal field evaporation source employing liquid gallium in a source configuration similar to that used in the electron emission studies exhibited a very large (ca. 10 to 100 μA) and stable ion current of Ga^+. This source looks very promising as a high brightness source of Ga^+ ions and will be investigated in greater detail.

ARPA Order No: 3164
Program Code No: 6D30
Name of Contractor: Oregon Graduate Center
Effective Date of Contract: May 14, 1976
Contract Expiration Date: August 15, 1977
Amount of Contract: $88,251
Contract No: F33615-76-C-1327
Principal Investigator: L. W. Swanson (Phone: 503-645-1121)
Project Engineer: J. M. Blasingame (Phone: 513-255-3732)
Contract Title: "Field Electron and Ion Source Research for High Density Information Storage System"
Reporting Period: May 14, 1976 - August 15, 1976

TABLE OF CONTENTS

LIST OF ILLUSTRATIONS

LIST OF TABLES

SECTION I

INTRODUCTION

This report describes progress made during the first 3 month period on a research program aimed at the development of high brightness charged particle sources suitable for use in information storage systems. In particular the charged particle source and focussing system envisioned for this application must be capable of providing a particle beam with sufficient flux density and smallness of size to address and/or read information at less than 0.1 μm resolution and at a rate of ~ 10^7 bits/sec. Because such requirements place a severe limit on the brightness requirements of the particle source, very few sources remain in contention as a viable option for such a memory system.

The primary aim of this research program is to evaluate high brightness field emission sources with respect to their potential for satisfying the above mentioned requirements for a particle source. In view of the fact that present high density archival memory schemes include both ion and electron beams this research will be examining field ionization (FI) as well as field electron (FE) sources. It is now established that FE and FI are the brightest sources presently available for electrons and ions respectively. Although considerable understanding and knowledge concerning the basic processes of FI and FE have been developed since their theoretical formulation some 50 years ago by Oppenheimer[1] and Fowler and Nordheim,[2] and their experimental embodiment pioneered by E. W. Müller,[3] many questions concerning their ultimate suitability as stable and long lived emitters remain.

Specifically this research is divided into the two following major tasks:

(1) Field Electron Source Development

and

(2) Field Ionization Source Development

In each task new source materials and modes of operation will be developed coupled with detailed evaluation of emission characteristic properties. In addition, some effort will be devoted to the further development of existing FE sources. The method of approach and specific measurements to be carried out will be given in greater detail in following sections of this and subsequent reports.

SECTION II

A CONSIDERATION OF FIELD EMISSION SOURCE OPTICS

The attractive feature exhibited by field emission sources in regards to their potential use in microbeam applications is their high brightness. An electron or ion beam brightness B at a given point in a given direction is defined as the current dI per unit area dA normal to the given direction, per unit solid angle $d\Omega$, that is

$$B = \frac{dI}{d\Omega dA} \tag{1}$$

It can be shown that a charged particle beam whose electric potential varies from V_1 to V_2 cannot increase the ratio of B_1/V_1 that is

$$\frac{B_1}{V_1} = \frac{B_2}{V_2} \tag{2}$$

which is the fundamental expression of the conservation of brightness. Thus, for a given Ω_2 the maximum rate at which information carried by a charged particle beam can be transmitted into a unit area of target at potential V_2 is determined by the brightness B_1 at the source.

Langmuir[4] showed that for a charged particle source exhibiting a semi-Maxwellian distribution of initial velocities the current density J at the image plane or at the beam crossover point is given by

$$J = \frac{J_o}{M^2}\left[1 - (1-x)\exp - [eV_2X/kT(1-x)]\right] \tag{3}$$

$(x = M^2\sin^2\theta$ and $0 \leq M\sin\theta \leq 1)$

where M is the overall magnification of the system, J_o, the current density at the source and θ, the semi angle of convergence in the image plane or at the beam crossover. The following two limiting forms of Eq.(3) can be obtained:

$$J = J_o \left(1 + \frac{eV_2}{kT}\right) \sin^2\theta, \quad x \text{ small} \tag{4}$$

$$J = \frac{J_o}{M^2}, \quad x \text{ large} \tag{5}$$

Physically the Langmuir equation gives the limit on the initial transverse energy E_{xy} a particle can have at the source and still be transmitted through a lens and arrive at a point on the image plane through a beam semi-convergent angle θ. It can be easily shown that this condition is given by

$$E_{xy} \leq E_2\left(\frac{x}{1-x}\right)$$

Since $eV_2/kT > 1$, Eq.(4) can be written in terms of the brightness B_2 at the image:

$$B_2 \cong \frac{J_o}{\pi} \frac{eV_2}{kT}, \quad x \text{ small} \tag{6}$$

An important question arises regarding the applicability of Eq.(3) for FE and FI sources since, the initial velocity distributions are not semi-Maxwellian. Worster[5] has shown that in general the axial brightness in a cylindrically symmetric system is given by

$$B_2 = \frac{J_o}{\pi}\left(\frac{eV_2}{\bar{E}_t} + \frac{\bar{E}_n}{\bar{E}_t}\right) \tag{7}$$

where $\bar{E}_t$ and $\bar{E}_n$ are the average initial transverse and normal energies of the emitting particles. Since $eV_2 >> \bar{E}_t$ the last term of Eq.(7) is negligible, giving

$$B_2 \cong J_o \frac{eV_2}{\pi \bar{E}_t} \tag{8}$$

Worster[6] goes on to show that the directional beam intensity at a given point off the optical axis is given by

$$B_2 = \frac{J_o eV_2}{\pi \bar{E}_t} \exp\ (-E_t/\bar{E}_t) \qquad (9)$$

where E_t is the initial transverse energy of the emitted particle. For $E_t = 0$ Eq.(9) becomes the expression for the axial brightness given in Eq.(8).

For Schottky and FE emission the values of $\bar{E}_t$ are[7]

$$\bar{E}_t = kT \text{ (Schottky)} \qquad (10)$$

$$\bar{E}_t = d \text{ (FE)} \qquad (11)$$

where

$$d \cong 9.75 \times 10^{-9} \frac{F}{\phi^{1/2}} \text{ (eV)} \qquad (12)$$

and where F and ϕ are the applied field strength (in V/cm) and the surface work function (in eV) respectively. For the usual current densities attainable d = 0.1 to 0.3 eV. In the paraxial region at the cross-over of a FE electron gun, Worster[6] shows that Eq.(9) becomes

$$B_2 = \frac{J_o}{\pi \bar{E}_t} \exp\ (-r^2/M^2a^2) \qquad (13)$$

where r, a and M are respectively the radial displacement at the cross over, the emitter radius and the gun magnification.

The Langmuir equations as expressed in the form of Eqs.(3) to (6) lead to several important observations. First, the maximum brightness and current density at the image plane is directly proportional to the source current density. Secondly, for a specified value of eV_2, there

exists a value of $M^2Sin^2\theta$ above which $JM^2/J_o \cong 1$. This means that all particles emitted from the source, regardless of their initial emission angle, reach the image. Fig. 1 gives plots of Eq.(3) for three values of $eV_2/\bar{E}_t$. For example, if $eV_2/\bar{E}_t = 10^5$ then $JM^2/J_o \cong 1$ for $M^2\sin\theta^2 \gtrsim 5 \times 10^{-5}$. Fig. 2 shows the values of M and θ for a specified value of $M^2\sin^2\theta$ and the values of the latter above which $JM^2/J_o \cong 1$ for various values of $eV_2/\bar{E}_t$. For example, if the value of $eV_2/\bar{E}_t = 10^5$ and M = 10, then, according to Fig. 2, $JM^2/J_o \cong 1$ for $\theta \gtrsim 7 \times 10^{-4}$ rad. On the other hand, if M = 0.01 then $\theta \gtrsim 0.7$ rad in order that $JM^2/J_o \cong 1$.

For a high brightness source with a small virtual size as is the case for FE and FI particle sources, a microprobe gun will operate near M = 1; thus, since θ generally exceeds 7×10^{-4} rad Eq.(5) appropriately gives the current density relationship between the source and image. In contrast a microprobe gun employing a Schottky source with its lower intrinsic brightness and accordingly larger virtual source size will operate at or below $M \cong 0.01$; thus for the usual range of $\theta < 0.1$ rad, the limiting form of the Langmuir Eq.(4) will give the current density relationship between source and image.

It should be emphasized that the above discussion gives the maximum current density at the image plane based on ideal (aberrationless) lenses. A real gun will, of course, be limited by the degree to which the probe forming optics system approaches the ideal case. A detailed discussion of the optimum probe forming optics and a comparison of Schottky and FE sources is given by Veneklasen.[8]

In the case of FE and FI sources the virtual source size is very small. Wiesner[9] has determined the virtual source size for an emitter shape approximated by the sphere-on-orthogonal-cone (SOC) model developed

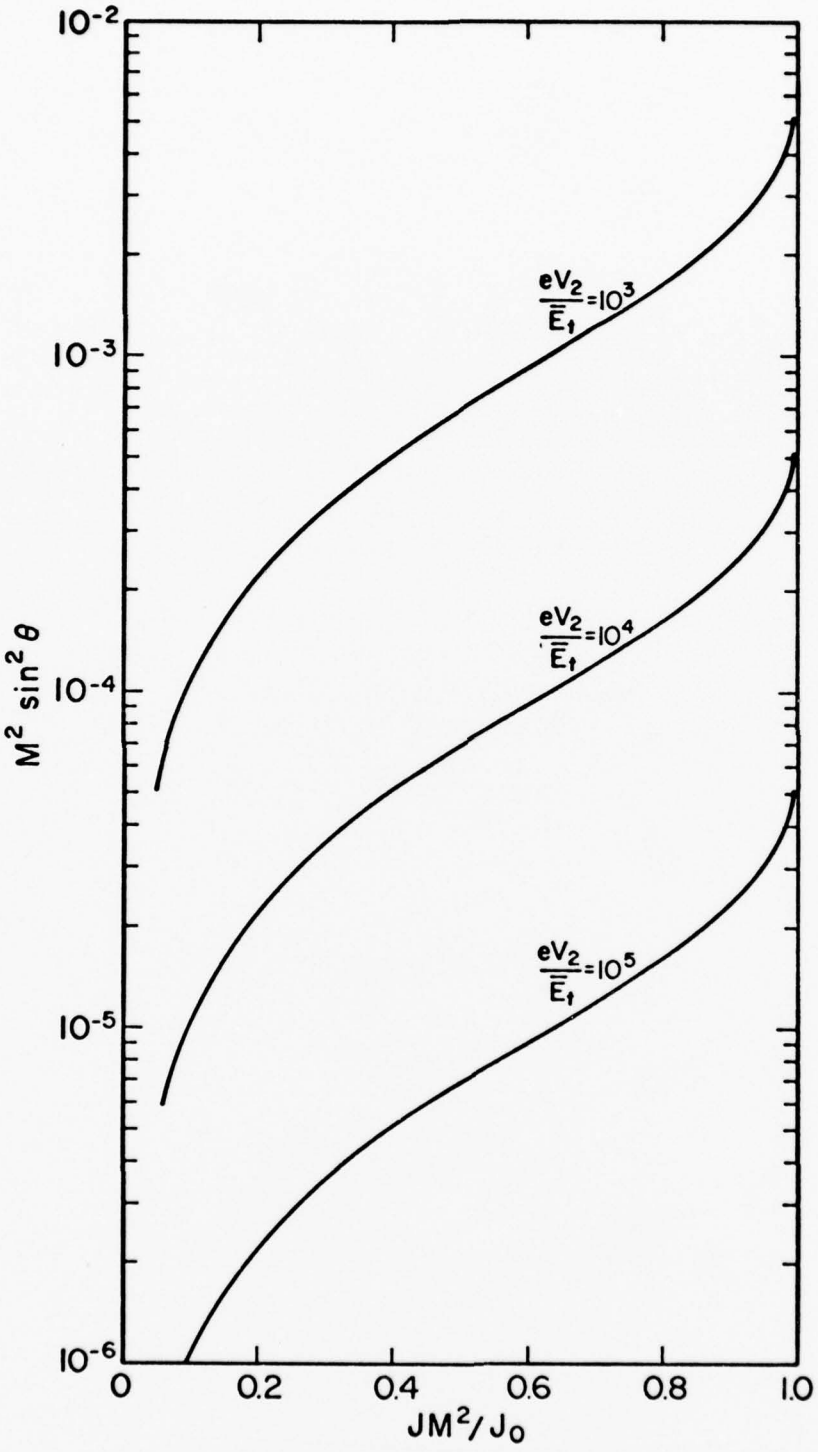

Figure 1. Plots of the Langmuir Eq.(3) for various values of eV_2/kT.

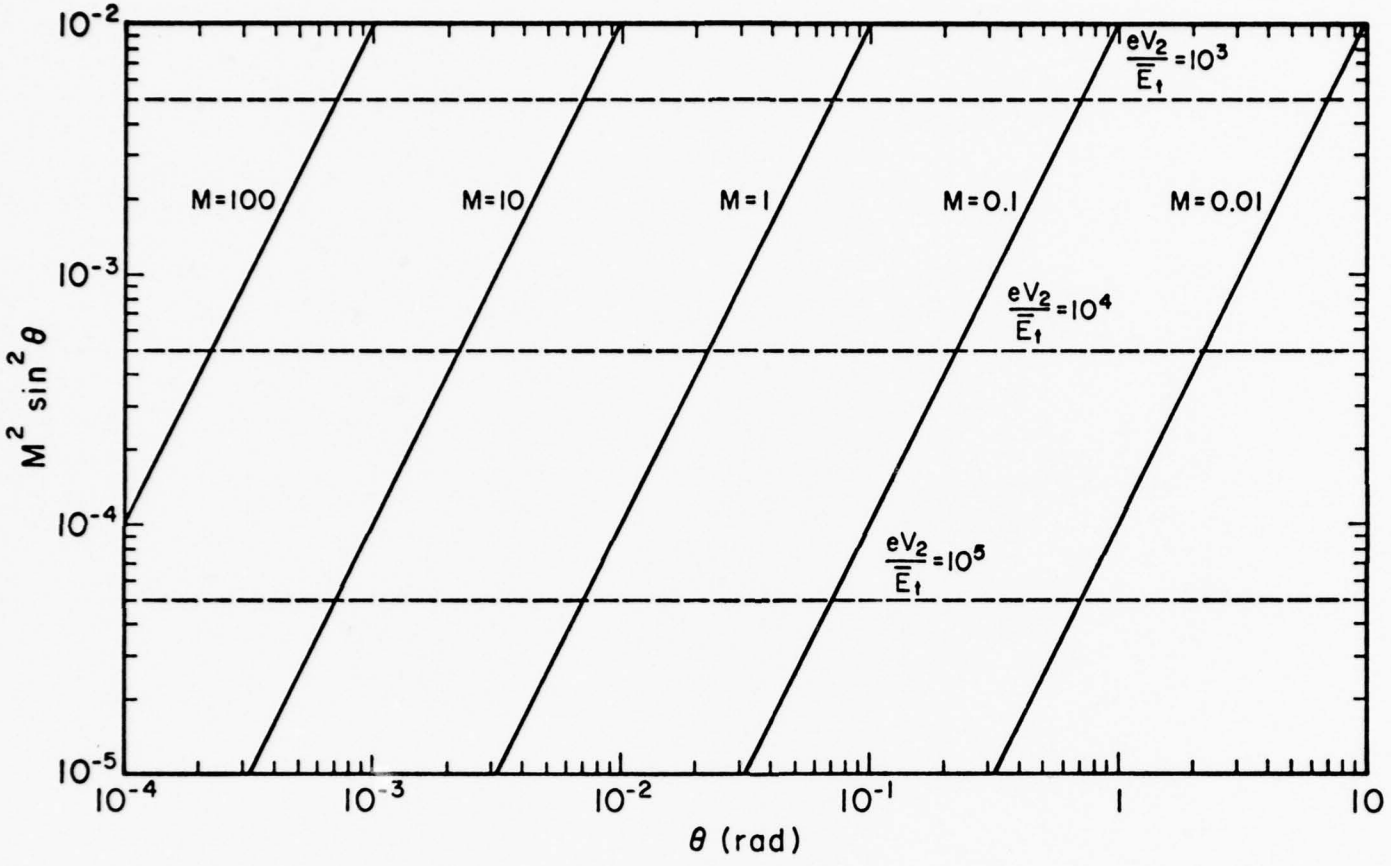

Figure 2. Plots of $M^2 \sin^2\theta$ vs θ for various values of M. The horizontal lines represent values of $M^2 \sin^2\theta$, for the indicated values of eV_2/kT, above which the Langmuir equation reduces to $J \cong J_o/M^2$.

by Dyke and coworkers.[10] Fig. 3 shows a diagram and relevant parameters of the SOC model. Based on this model, equipotential surfaces $V(\rho,\theta)$ depicting a particular emitter shape are generated by

$$V(\rho,\theta) = V_R\left(\frac{r_o}{R}\right)^n \left[\left(\frac{\rho}{r_o}\right)^n - \left(\frac{r_o}{\rho}\right)^{n+1}\right] P_n(\cos\theta_o) - V_{oo} \qquad (14)$$

where V_{oo} is the potential of the emitter surface relative to the SOC, V_R is the potential on an anode a distance R from center of the sphere and $P_n(\cos\theta)$ is the Legendre function of index n. The value of n, which varies from 0.1 to 0.5 for typical emitter shapes establishes the exterior cone angle θ and is determined by the condition that $P_n(\cos\theta_o) = 0$. Fig. 4 gives the relationship between n and θ_o for the latter condition. The value of V_{oo} is given by

$$V_{oo} = V_R\left(\frac{r_o}{R}\right)^n \left[\gamma^n - \gamma^{-n-1}\right] \qquad (15)$$

where $\gamma = \rho_{oo}/r_o$. The degree of "necking" of the emitter (see Fig. 3) is determined by γ - larger values of γ cause less necking of the emitter shape. Typically, the range of n and γ are 0.1 to 0.4 and 2.0 to 3.0 respectively. Based on Wiesner's results, Figs. 5-7 give the respective source sizes for typically shaped FE and FI sources of varying radii and aperture half angle. The smaller size of the FI source is due primarily to a negligible $\bar{E}_t$ at the low operating temperature of the source and the smaller diffraction limit of a proton beam. Because of their small virtual source size, probe forming guns using field emission sources need not be highly demagnifying thus only one or, at most, two lenses are required. Compared with conventional sources the field emission source requires a relatively simple optics system.

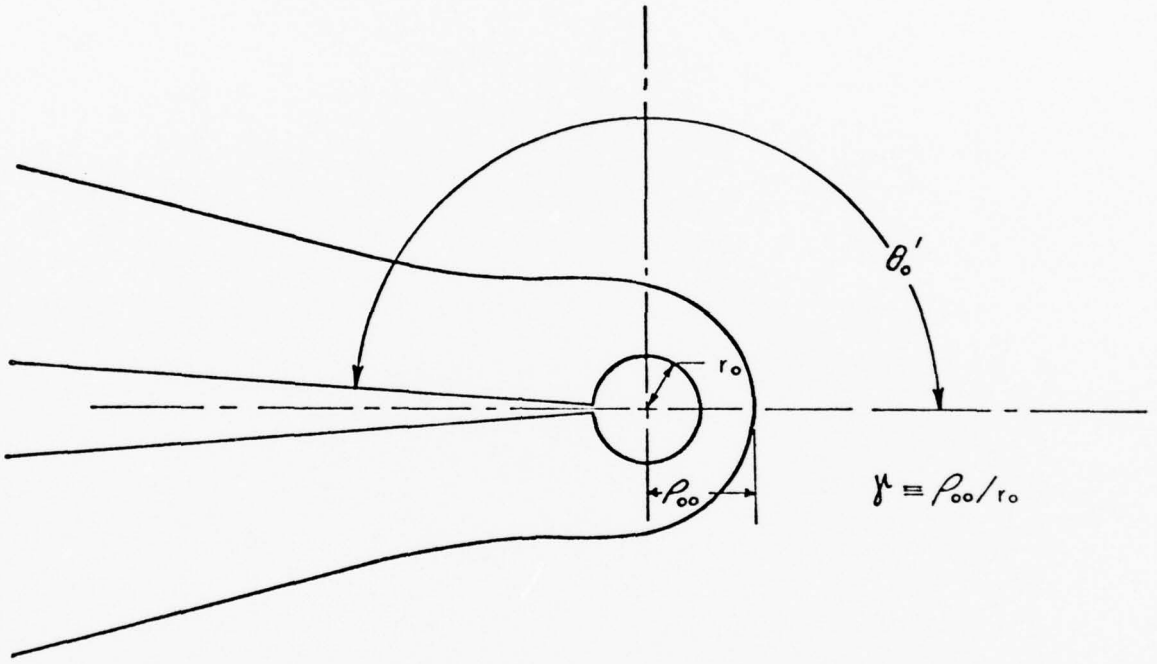

Figure 3. The sphere at the end of the orthogonal cone model depicted in this figure is capable of generating equipotentials which closely approximate those generated at the surface of a typical field emitter (shown in figure as the profile surrounding the model).[10]

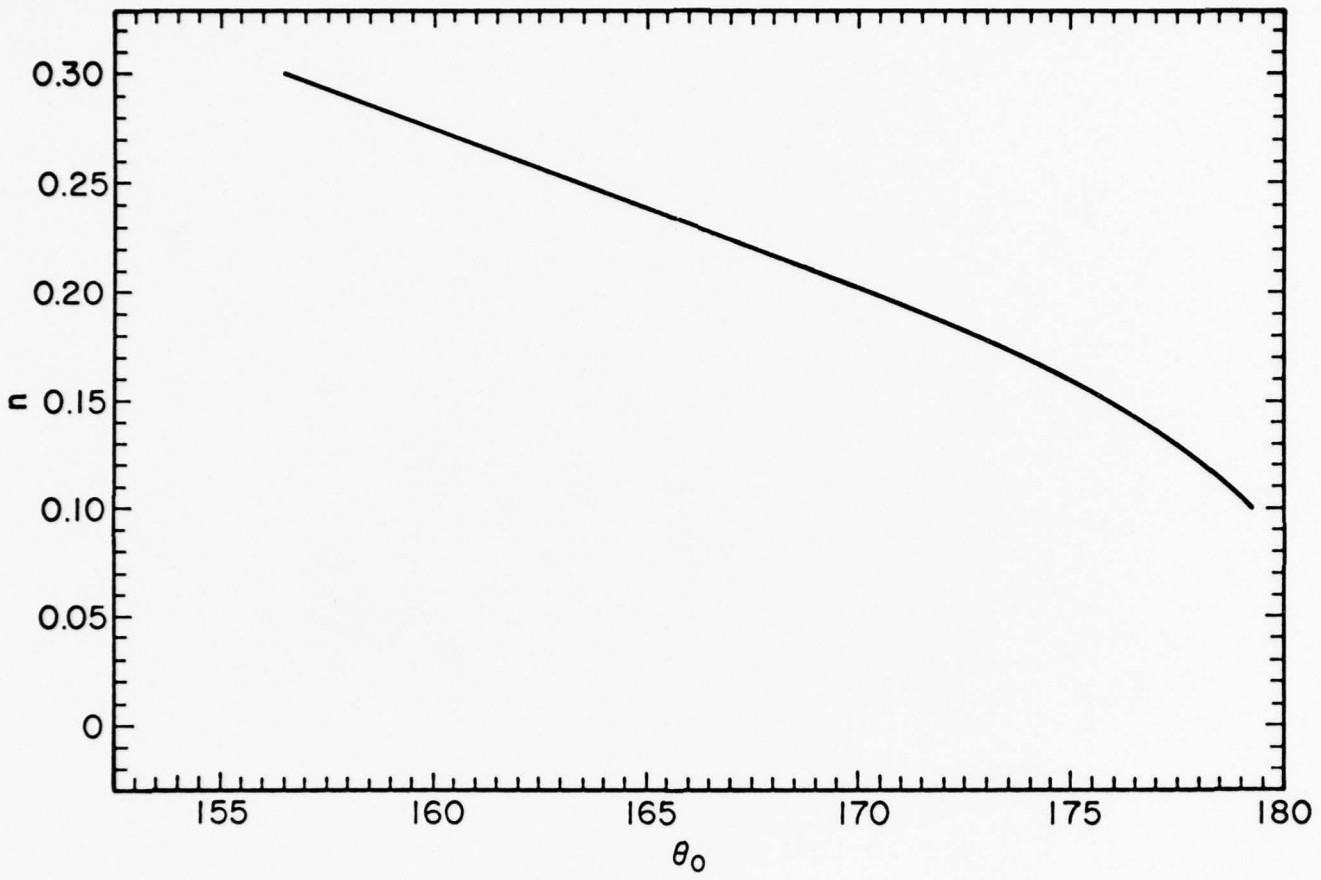

Figure 4. Relationship between n and θ_o for which Pn ($\cos\theta_o$) = 0.

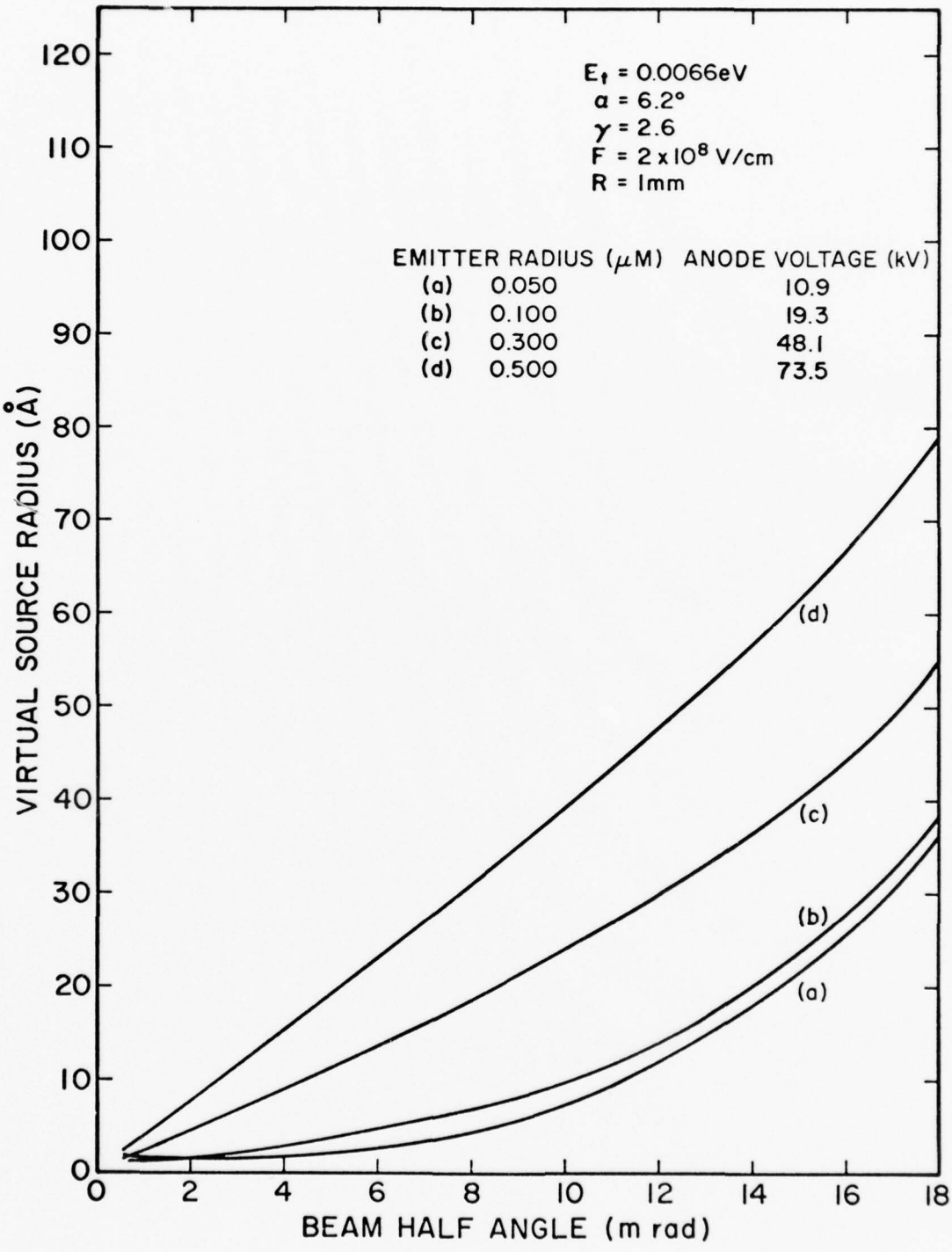

Figure 5. Virtual source size vs beam half angle for a FI source of H^+ ions using SOC model and aberration terms computed by Wiesner.[9] Source temperature assumed to be 77 K.

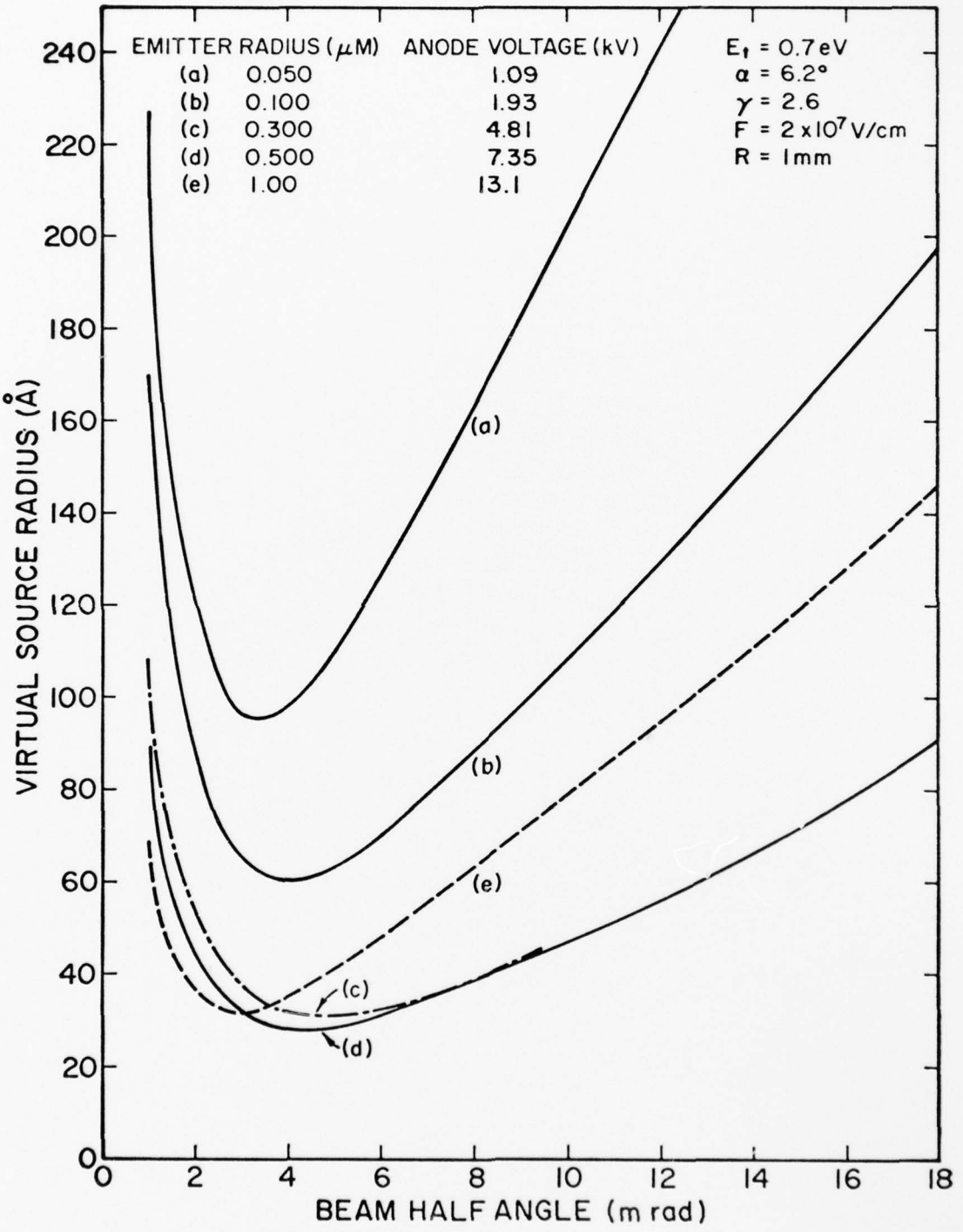

Figure 6. Virtual source size vs beam half angle for FE source at $F = 2 \times 10^7$ V/cm using SOC model and aberration terms computer by Wiesner.[9]

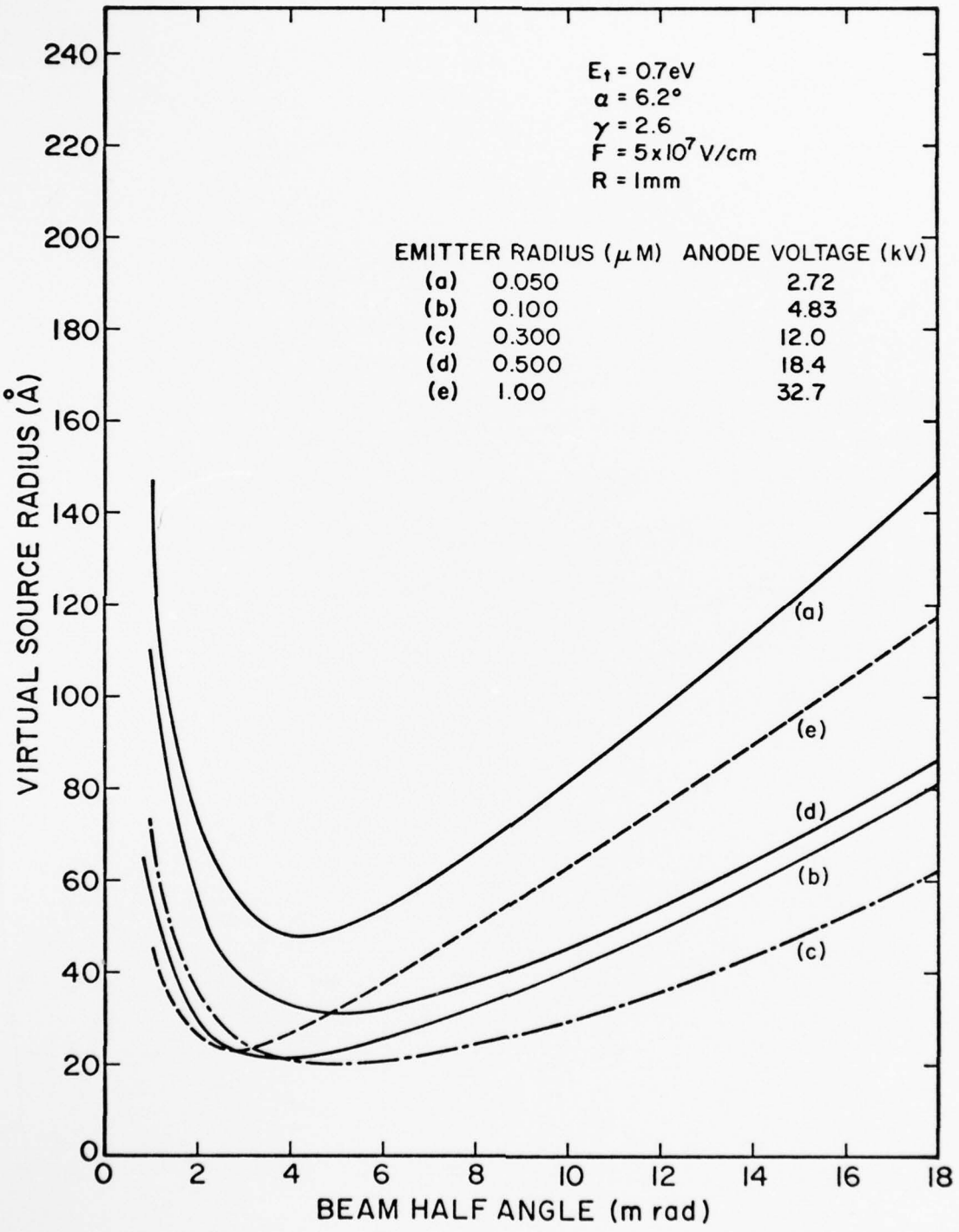

Figure 7. Virtual source size vs beam half angle for FE source at F = 5 x 10^7 V/cm using SOC model and aberration terms computed by Wiesner.[9]

For small angles θ the current that diverges into a solid angle $\pi\theta^2$ from a virtual source ρ_s is given by

$$I = \frac{dI}{d\Omega}\,\pi\theta^2 \tag{16}$$

or

$$B_1 = \frac{dI/d\Omega}{\pi\rho_s{}^2} \tag{17}$$

The range of values of $dI/d\Omega$ for an operational FE source extend from 1×10^{-4} A/Sr for room temperature operation to 1×10^{-3} A/Sr for thermal field TF operation. If a value of 30 Å is assumed for ρ_s the source brightness can be determined to be in the range 10^8 to 10^9 A/Sr cm^2. In the case of a gas supplied FI source a maximum angular intensity of 1×10^{-6} A/Sr can be obtained.[11] Based on Fig. 5 values of ρ_s a maximum source FI brightness of 10^7 to 10^8 A/Sr cm^2 can be expected.

Table I summarizes the emission characteristics for several particle sources. The FE and FI sources are clearly superior when high brightness is required. However, because of the relatively small values of both $dI/d\Omega$ and ρ_s field emission sources are only suitable when small focussed beam spot sizes are required. Generally, the field emission sources are superior to all other sources of ions or electrons when the focussed spot size is less than ~ 5000 Å. In addition, because field emission sources exhibit a smaller energy spread than conventional ones, the spot size limit due to chromatic aberration is greatly reduced.

It is interesting to note from the results shown in Figs. 6 and 7 that the smallest FE virtual source size for the SOC model occurs for emitter radii between 0.3 and .5 μm. This is in contrast to a spherical emitter where the source size is directly proportional to emitter radius.

TABLE I

TYPICAL CHARACTERISTICS OF VARIOUS ELECTRON SOURCES

Source	Angular Brightness (A/Sr)	Approximate Source Size (μm)	Brightness (A/cm^2 Sr)	Energy Spread (eV)
FE	3×10^{-5}	.003	1×10^{8}	.2
Thermal FE	3×10^{-3}	.003	1×10^{10}	.8
LaB_6 Schottky Cathode	$\sim 10^{-1}$	1	$\sim 10^{6}$	.2
FI	1×10^{-6}	.001	1×10^{8}	2-5
Duoplasmatron	-	1000	10^{4}	10

The larger source size at small emitter radii for the SOC model is due to an increase in diffraction and chromatic aberration contribution for lower voltage emitters.

By differentiating Eq.(15) the field strength F at the emitter apex can be determined to be

$$\beta = \frac{F}{V_R} = \frac{r_o^{n-1}}{R^n} \left[n\gamma^{n-1} + (1+n)\gamma^{-2-n} \right] \qquad (18)$$

The above expression was used to calculate the anode voltages to give the indicated field strengths listed in Figs. 5-7. For values of R = 0.1 to 1 cm an approximate value of β is given by

$$\beta = 0.6/\rho_{oo}^{.87} \; R^{0.13} \; \alpha^{.33} \; (cm^{-1}) \qquad (19)$$

where $\alpha = \pi - \theta_o$ is the cone half angle of the emitter. Figs. 8 and 9 show plots of Eq. (17) for typical emitter shapes. The field factor β increases with decreasing ρ_{oo}, R or α. Emitter radii between .05 and 1.0 μm can be obtained by standard fabrication procedures.

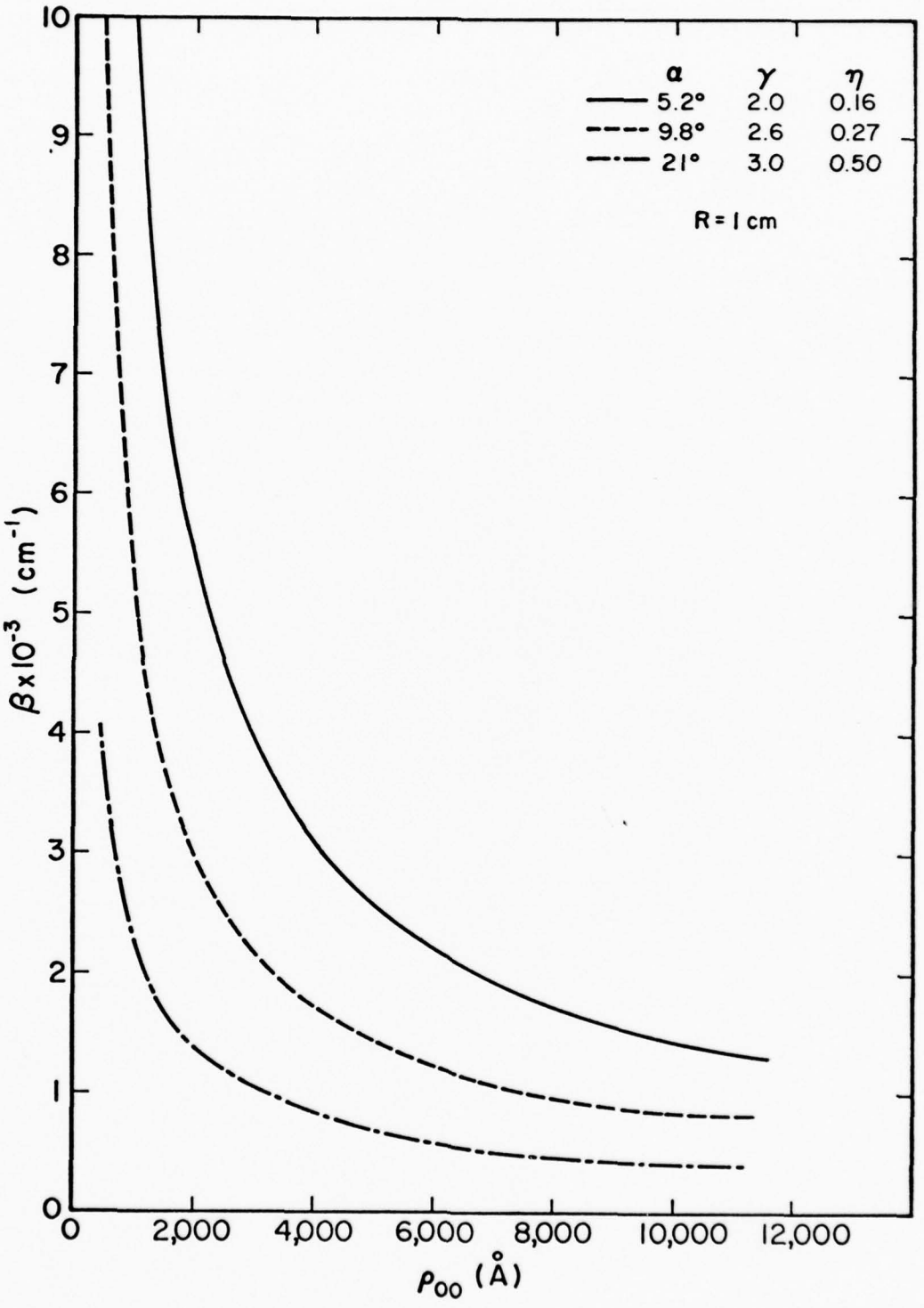

Figure 8. Field factor β vs apex radius ρ_{00} for a SOC model.

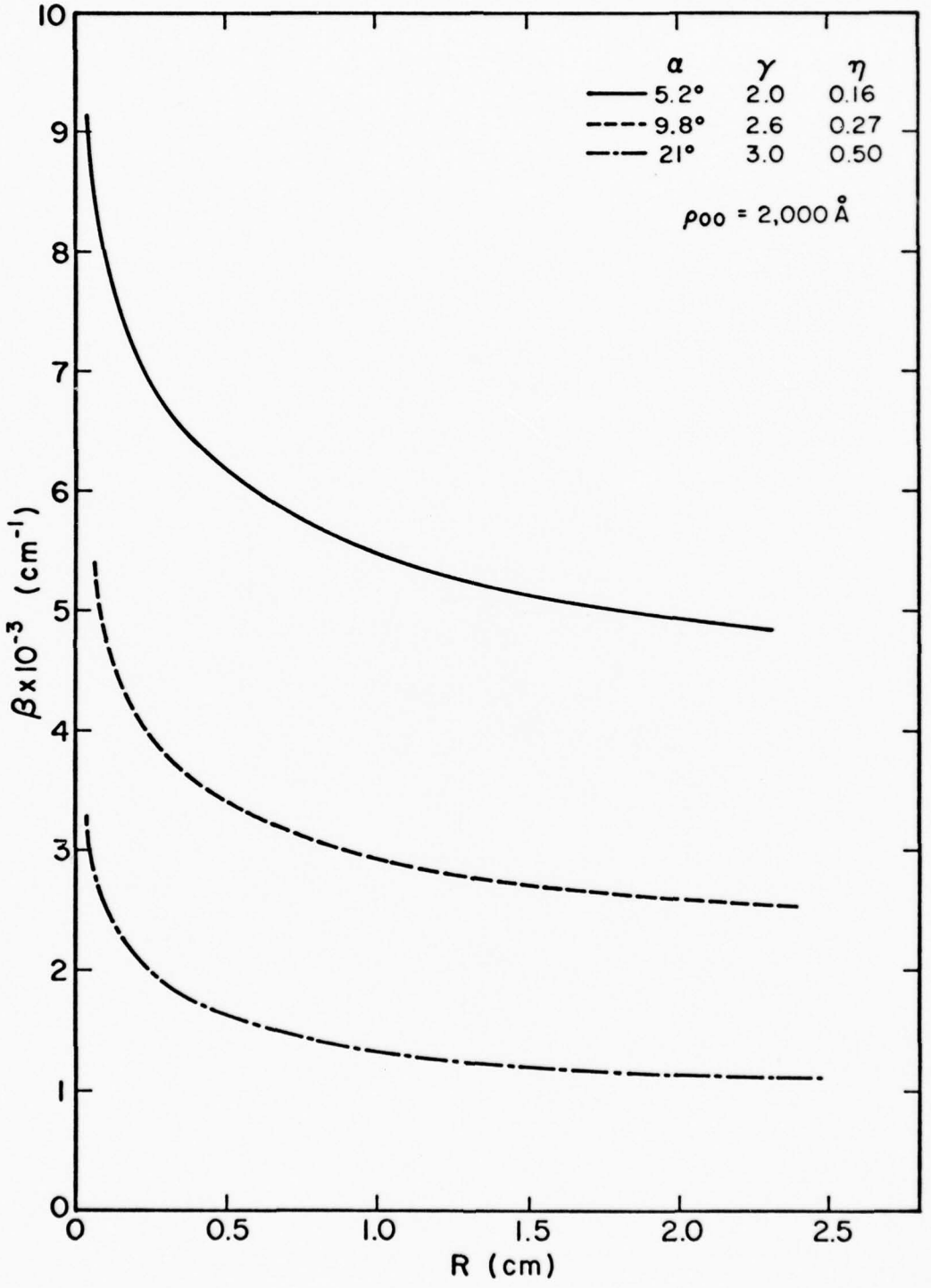

Figure 9. Field factor β vs emitter-to-anode spacing for a SOC model.

SECTION III

EMITTER MATERIALS FABRICATION

The physical properties desirable for an emitter material are 1) high tensile strength to withstand electrostatic stresses, 2) high resistance to sputtering and contamination and 3) high melting point to permit thermal cleaning. Possible materials possessing these properties can be divided into three categories: 1) pure metals, 2) heterogeneous cathodes consisting of a surface layer on a solid substrate, and 3) homogeneous metalloid compounds and alloys.

Of the pure metal materials investigated in the past which satisfy the above requirements, tungsten operated at room temperature or in the thermal-field (TF) mode has proved to be the most suitable material. TF mode operation has worked successfully with (100) oriented tungsten emitters by allowing electrostatic induced geometric change to reshape the emitter to a particular end form that is stable at elevated temperatures.[11,12] The mobility of the surface atoms at high temperature causes cathode sputtering damage to instantly heal thereby maintaining a smooth and clean surface that exhibits stable emission.

The zirconium coated tungsten cathode, also operated in the TF mode, is an example of a heterogeneous cathode that has proved to be a practical emitter.[11-13] Resupply of the Zr sputtered from the emitter apex occurs by surface diffusion from the emitter shank.

A. Tungsten Emitter Fabrication

Two procedures leading to slightly altered emitter shapes have been developed in the past to form emitters from tungsten. Both procedures involve immersing a short length of single crystal tungsten wire spot welded to a .13 mm diameter W heating filament into a solution of

2N NaOH. The dimensions of the single crystal W blank are ~ 2 mm in length (as measured from the point of spot weld) by .13 mm in diameter. Electrochemical formation of the emitter tip can be accomplished by applying a continuous a.c. voltage of 13 V or a d.c. voltage (emitter positive) of 9 to 13 V. The former is called the a.c. self termination technique and the latter the d.c. drop off technique. In the case of the a.c. method the emitter formation continues until the emitter recedes from the solution, thus terminating the process. The d.c. technique is terminated by quickly (within a few μsec.) switching off the etching voltage when the lower portion of the immersed emitter blank separates from the blank due to the etching action.

Fig. 10 shows typical emitter shapes formed by the two processes. Table II gives the typical range of emitter cone half angle and radius obtained by the respective procedures. Larger cone angles and emitter radii are formed by the a.c. process.

TABLE II

GEOMETRICAL CHARACTERISTICS OF W EMITTERS FORMED BY TWO PROCESSES

Process	Emitter Cone Half Angle (Deg)	Emitter Apex Radius (μm)
a.c. self termination	4-6	.02 - .05
d.c. drop off	8-10	.13 - .16

Fig. 11 shows an a.c. processed emitter just after being formed (a) and then after thermal cycling to 1600 K (b). A slight necking of the emitter can be observed in Fig. 11(b) after the thermal processing.

Studies thus far show that emitter shape and radii in the range indicated in Table II can be routinely produced by these two processes.

(a) (b)

Figure 10. Photographs of the typical shape of a field emitter formed by the a.c. self termination (a) and d.c. drop off (b) techniques.

(a) (b)

Figure 11. Emitters formed by a.c. self termination process ($M = 38 \times 10^3$ X); (a) before and (b) after thermal cycling to 1600 K.

Future studies will be aimed at developing procedures to fabricate emitter radii in the range of 0.2 to 0.6 μm.

B. Tungsten/Zirconium Emitter Fabrication

In the past Zr has been deposited on the emitter by in situ evaporation or by depositing an organic solvent slurry of ZrH_2 on the emitter mechanically and thermally diffusing the free Zr to the emitter apex.[14] Both methods have provided long lived cathodes and have certain advantages. The vapor deposited method can be carried out quite reproducibly compared with the mechanical method. On the other hand, the latter technique is relatively quick and simple to perform. Other techniques, such as electrolytic and sputter deposition are being examined.

C. Rare Earth Boride Emitter Fabrication

The borides and carbides of certain transition and rare earth metals are believed to be more durable emitter materials than tungsten because of their high tensile strength and resistance to sputtering. Although preliminary studies of the FE characteristics of this class of emitter materials were carried out many years ago by Elinson et al,[15] successful FE cathodes were not developed primarily because of material difficulties. More recently, an LaB_6 FE emitter has been reported to operate for more than 1000 hrs. at room temperature and at a current level of 1 to 2 mA.[16] Such a high current level is difficult to sustain even for tungsten in TF mode operation.

In recent work in this laboratory a simple and reliable method of fabricating high purity single crystal needles of LaB_6, SmB_6, and CeB_6 has been developed.[17] This has removed one of the major barriers

impeding previous investigation of RB_6 (R = rare earth) emitters, i.e. the fabrication of pure and homogeneous single crystal material. The method employed, first performed by P. Lebeau and J. Eiguras,[18] later by Aito, et al[19] for LaB_6 is referred to as the "molten flux" method of single crystal growth. The method consists of mixing stoichiometrically the basic elements of the boride compound, e.g. powdered B and metallic rare earth metal, in an inert crucible and heating in an argon atmosphere to ~ 1500°C. After cooling the solid Al solvent was dissolved with warm HCl leaving needle and plate-like single crystals of the boride compound. The details of the fabrication procedures and results for La, Ce and SmB_6 are given below.

1. Single Crystal Fabrication Procedures

The starting materials in our application of this method consisted of 60 mesh boron powder, ingot formed aluminum, and metallic chips of the rare earth metal. Table III lists typical impurity levels for the starting materials used in the single crystal preparation.

TABLE III

BULK PURITY SPECIFICATIONS OF THE VARIOUS MATERIALS MEASURED BY OPTICAL EMISSION SPECTROGRAPHIC TECHNIQUES

Material	Impurities (ppm)											
	Si	Mg	Fe	Cu	Al	Ca	Ni	O	C	Ag	Eu	Nd
Aluminum	3	<1	2	1	<1	<1	<1	-	<1	<1	-	-
Lanthanum	300	-	300	-	300	500	300	-	-	-	-	-
Boron	<20	<20	250	<20	<20	<20	<20	100	300	-	-	-
Samarium	<100	-	100	<100	<100	<100	-	-	-	-	500	300
LaB_6*	100	100	<10	<10	-	100	<10	-	-	100	-	-

*single crystals prepared

The single crystal growths were performed in 30 ml alumina boats placed in a resistively heated silicon carbide globar horizontal tube furnace. The boron was placed in four 4.8 mm diameter holes bored in the aluminum ingot and the rare earth was placed on the top center of the ingot. Before each run the growth chamber was evacuated and back-filled to one atmosphere pressure with high purity argon. The heating rate was from room temperature to 1500°C over a period of 6 hours and maintained at 1500°C for 8 hours. Cooling from 1500°C to 800°C took place at the conductive cooling rate of the furnace over a period of 1.5 hours; further cooling to room temperature occurred conductively over a 2 hour period.

After dissolving the Al solvent with HCl large single crystal platelets (approximately 2 mm square by 0.1 mm and some 1 x 7 x 0.1 mm) formed. Cubic shapes also 1 to 2 mm on a side were also observed. In addition, needle shapes 6 to 8 mm long and 0.1 to 0.2 mm square cross section were produced. A typical selection of these crystal shapes are shown in Fig. 12. Similar results were obtained with Ce.

2. Single Crystal Evaluation

Optical emission spectrographic analysis of the prepared LaB_6 single crystals indicated, according to the Table III summary, that crystal purity was superior to the starting materials. Subsequent Auger spectroscopy surface analysis of the crystals after flashing at ~ 1600 K showed only La and B. Apparently even the Al solvent is not appreciably incorporated into the growing crystals of LaB_6.

X-ray diffraction pictures of the platelet surface shown in Fig. 13 indicate a (100) direction perpendicular to the platelet face.

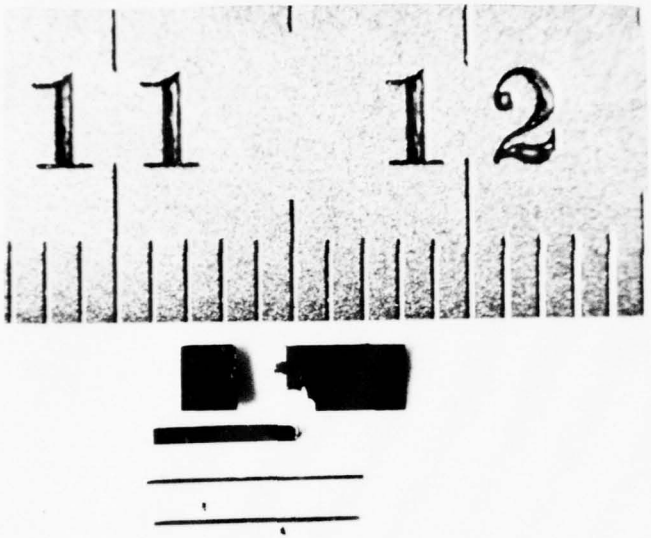

SmB_6 Size

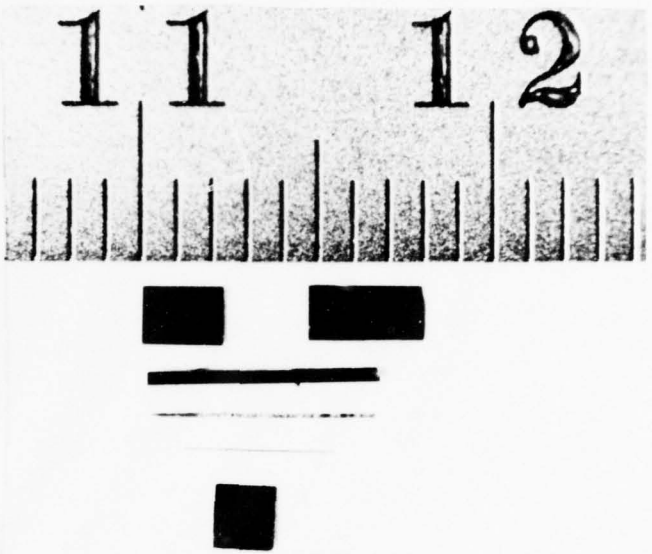

LaB_6 Size

Figure 12. Typical shapes and sizes of the LaB_6 and SmB_6 single crystals produced by the liquid aluminum flux technique.

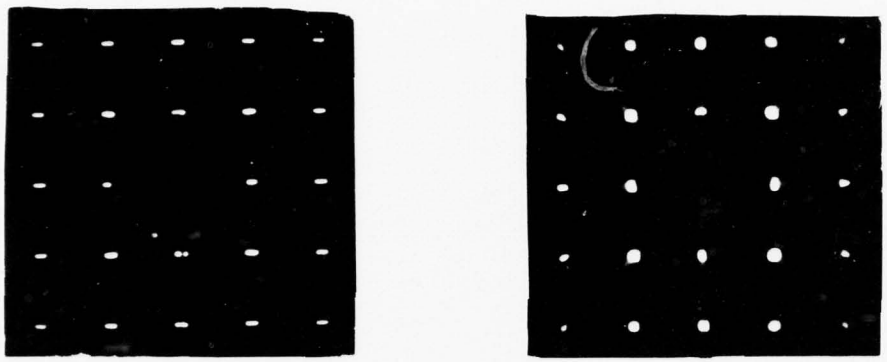

(a) (b)

Figure 13. X-ray diffraction patterns of (a) the longitudinal face of a LaB_6 needle shape crystal and (b) the face of a LaB_6 single crystal platelet.

X-ray diffraction of the longitudinal faces of the needle structures gave (100) and (110) faces. Thus the needle axis, which is the growth direction, is probably a (110) direction. The sharpness of the x-ray diffraction spots indicate relatively defect free single crystal specimens.

From powder x-ray diffraction patterns a lattice constant for the LaB_6 crystals of 4.156 Å was obtained; this is in excellent agreement with the literature value of 4.157 Å.[20] Similar x-ray examination of the prepared SmB_6 crystals gave a lattice constant of 4.132 Å also in good agreement with the literature value of 4.129 Å.[20]

In summary, we conclude that the liquid metal flux technique of forming small single crystals of LaB_6, CeB_6 and SmB_6 is successful. It is our expectation that several other rare earth hexaboride compounds which exhibit congruently melting hexaborides, such as PrB_6 and NdB_6 will form single crystals by this technique.

3. Emitter Fabrication

Emitters were quickly and conveniently prepared by mounting the needle shaped single crystal blanks on a flat rhenium ribbon (0.001" x 0.010") and fixed to it by means of a spot-welded rhenium strap of the same thickness and width (see Fig. 14). In addition, a binder of $MoSi_2$ was inserted between the emitter and rhenium support strap. The emitter points were obtained by electrochemical etching in a 50% methanol/NaOCl solution at 1.5 V. The power requirements to resistively heat the emitter shown in Fig. 14 to ~ 1800 K are less than 3 watts.

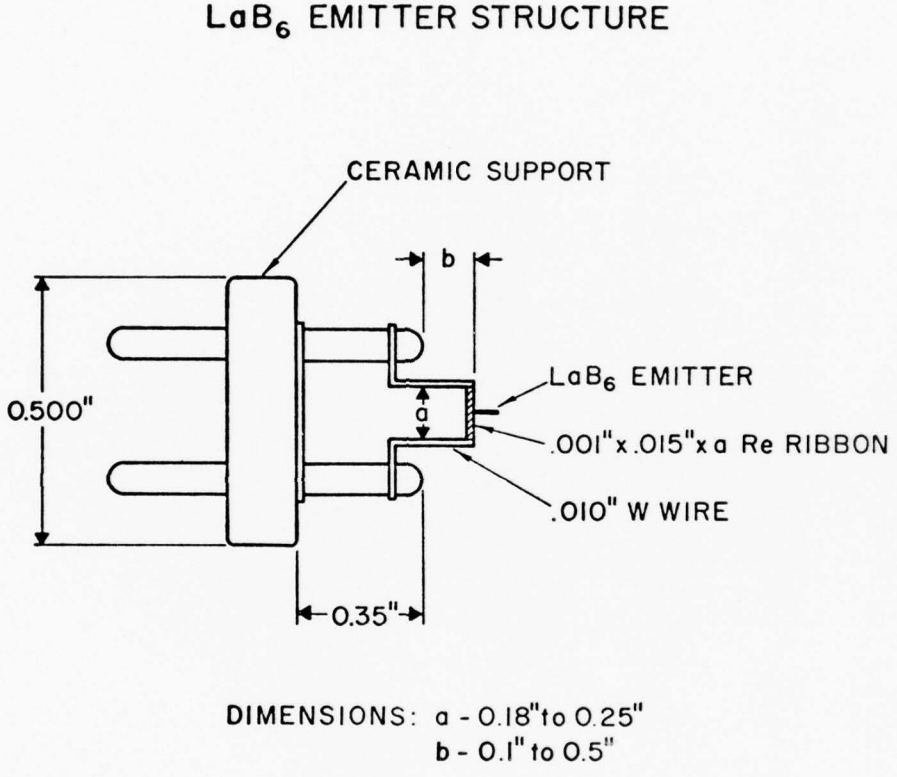

Figure 14. Diagram of emitter and resistively heatable filament support structure used for single crystal material of LaB_6.

Highly magnified photomicrographs of a LaB_6 emitter are shown in Fig. 15 for three rotational orientations of the emitter. The gross diameter of the emitter end form is about 1000 Å; however, close inspection of the photomicrographs reveals that the emitter has a built-up end form with a diameter at the apex of only 100 Å. The built-up feature is due to the application of the d.c. field while heating in vacuum. Field induced migration of the substrate occurs which causes preferential development of certain planes. This effect is a well known phenomenon[21] and has been used to advantage in the development of practical field emission cathodes[11,12] for which it is an advantage to have electron emission confined to a narrow cone about the emitter axis.

Similar shaped emitters have been fabricated from the single crystal needles of CeB_6 and SmB_6. Further studies aimed at preparing emitters of specific radii are being continued.

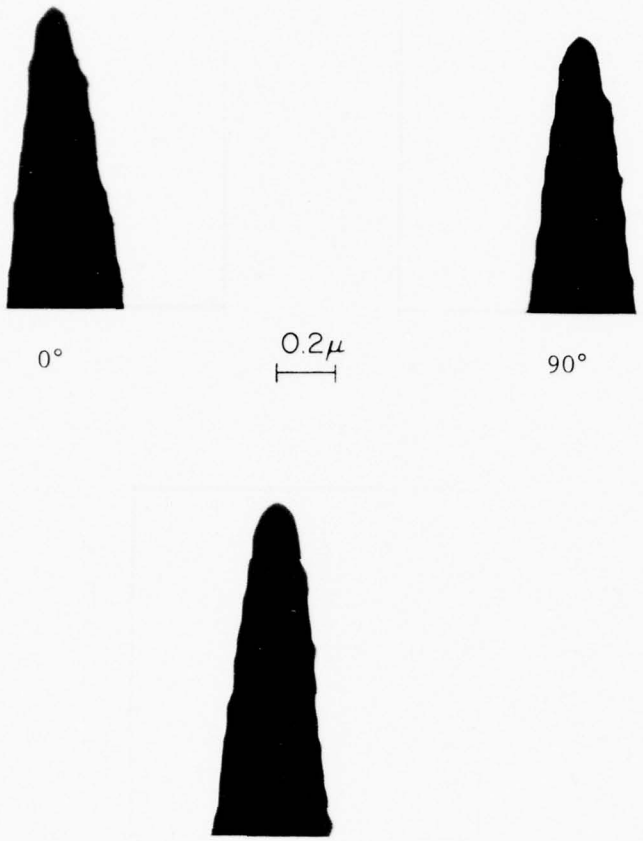

Figure 15. Micrograph profiles of an LaB_6 field emitter which has been operated in a TF mode.

SECTION IV

ELECTRON EMISSION STUDIES

Preliminary studies of the field emission characteristics of LaB_6 single crystals have been carried out. Difficulties have been encountered in obtaining reproducible and coherent patterns. In many cases emission seemed to be occurring from randomly spaced emission points on the emitter surface.

Fig. 16 shows the emission pattern from an LaB_6 emitter after several temperature cycles above 1800 K. These patterns were obtained from the same emitter as shown in Fig. 15. The overlapping circles of emission can only be explained in terms of small (atomic sized) protrusions on the emitter surface which preferentially emit due to local field enhancement. The overlapping circles of emission were observed to change position with temperature cycling.

The aforementioned results were usually observed with low voltage ($V < 1000$ volts) emitters. It was speculated that the erratic behavior of the previous emitters were due to stoichiometry variations at the emitter surface due either to a bulk stoichiometry differing from $\frac{La}{B} = \frac{1}{6}$ or to a preferential evaporation of lanthanum or boron. To avoid this possibility subsequent emitter blanks were maintained at high temperatures for several hours prior to forming the tip.

Fig. 17 is a sequence of FEM patterns obtained from a higher voltage LaB_6 emitter. Photos (a) and (b) were taken during the thermal cleaning sequence. From Auger spectroscopy studies it was determined that heating the LaB_6 crystals to 1700 K resulted in a clean surface. An interesting observation in the Fig. 17 photos is the reversal in emission distribution

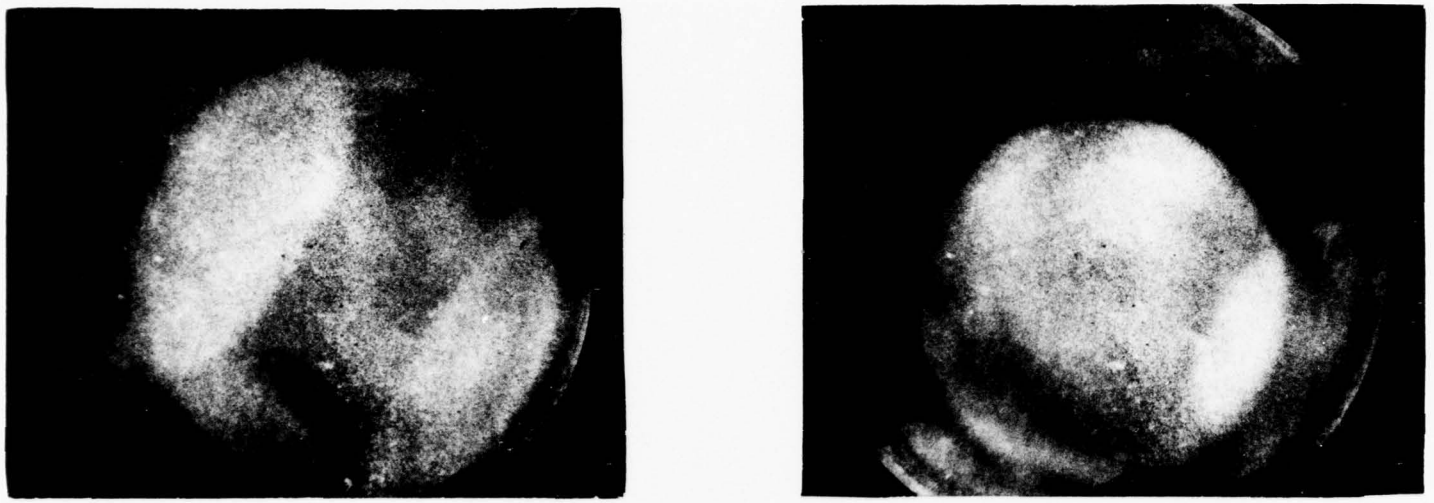

(a) (b)

Figure 16. Pulsed field electron patterns obtained from the Figure 15 emitter. Photo (a) was obtained after initial thermal cleaning; photo (b) was obtained after prolonged thermal cycling and operating in the TF mode.

(a) V = 1800 V (d.c.)

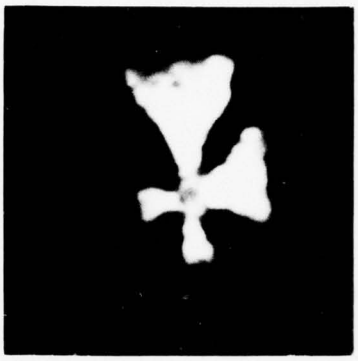

(b) V = 4900 V (d.c.)

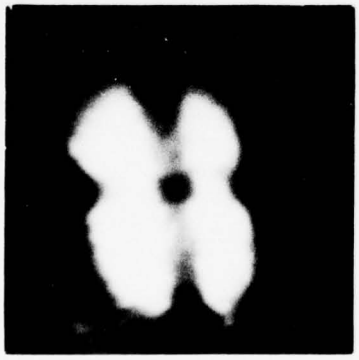

(c) V = 8 kV (Pulse)

(d) V = 8 kV (Pulse)

Figure 17. Field electron microscope patterns of an LaB_6 emitter; (a) and (b) were during the early stages of thermal cleaning and taken with a d.c. applied voltage; patterns (c) and (d) were taken during the latter stages of thermal cleaning using a pulse viewing voltage. The (110) plane is the central plane.

between (b) and (c). Photos (c) and (d), which are believed to be clean surfaces, show a definite 2-fold symmetry characteristic of a (110) orientation along the emitter axis. It is also clear from the latter photos that the (110) plane (in the center of the pattern) is a high work function. From the pattern symmetry it can be concluded that the (100) planes, located on the top and bottom of photo (c), and the (111) planes, located on the right and left side of the (110) plane, are also high work function planes.

As an electron optical source it is desirable to have the lowest low work function plane along the emitter axis. It appears the lowest work function region occurs in the center of the triangle formed by the (110), (111) and (100) directions.

Future work on emitter fabrication will be aimed at developing zone refining and crystal seeding techniques in order to obtain specified crystal directions along the emitter axis.

The current-voltage relationship from the Fig. 15 LaB_6 FE emitter is shown in Fig. 18 in the form of the well known Fowler-Nordheim (FN) plot. The Fowler-Nordheim equation describing the field electron current-voltage relationship is given by

$$J = \frac{1.54 \times 10^{-6} F^2}{t(y)} \exp\left(-6.83 \times 10^7 \phi^{3/2} v(y)/F\right)(A/cm^2) \qquad (20)$$

if F is in V/cm and ϕ in eV. The correction terms t(y) and v(y), which are due to the image potential, are tabulated[22] slowly varying functions of the auxiliary variable $y = (e^3F)^{1/2}/\phi$. If a value of $\phi = 2.4$ eV is assumed, a value of $\beta = 1.5 \times 10^4$ cm^{-1} was obtained from the linear portion of the Fig. 18 plot. The apparent deviation of the I(V) data from

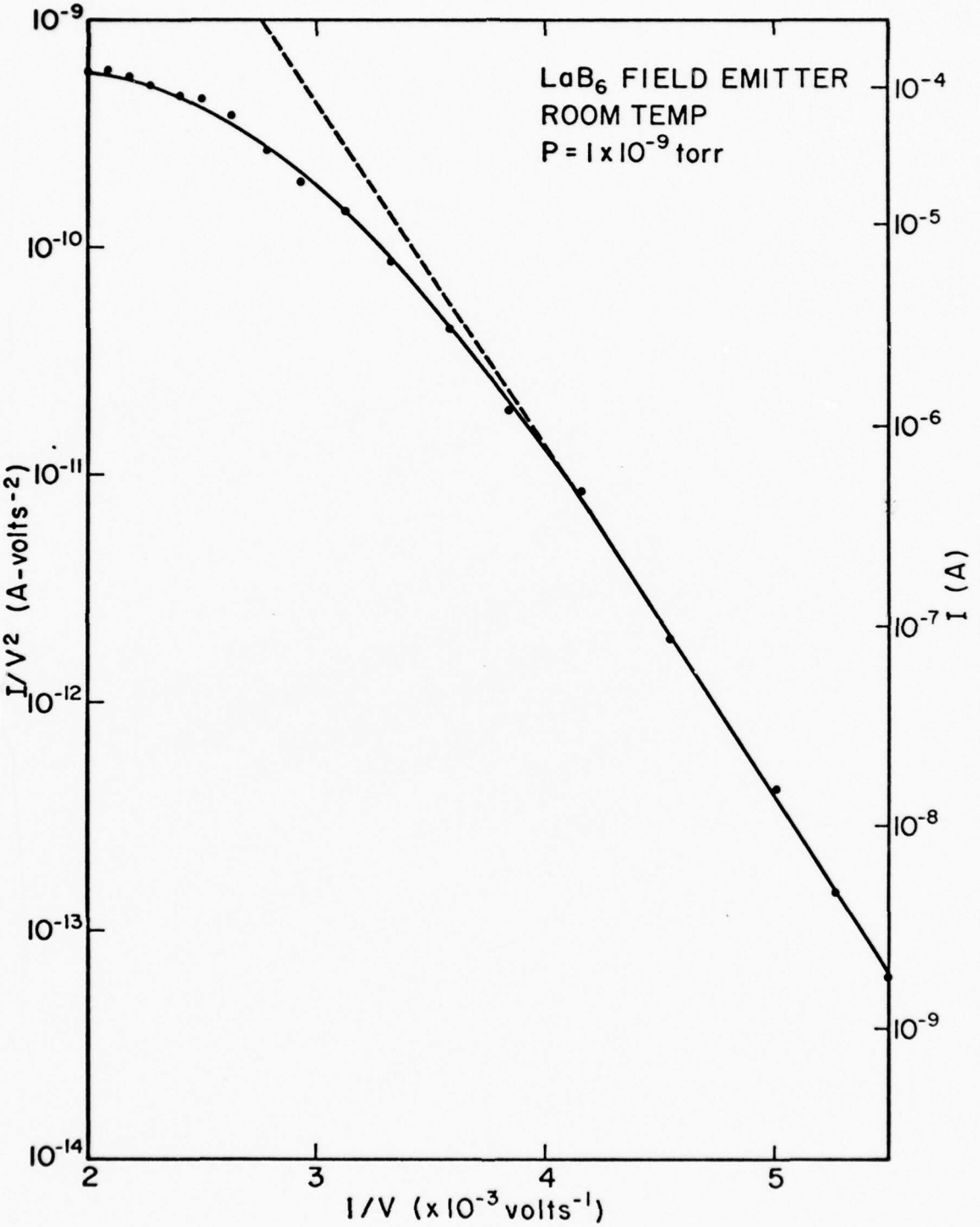

Figure 18. A room temperature FN plot of the I(V) data taken for the LaB_6 emitter shown in Figure 19.

the FN plot in Fig. 18 is, at least in part, due to space charge. Further studies are being conducted to ascertain the exact contributions of space charge and other effects in the observed experimental results.

Emission currents as high as 1.0 mA have been obtained from a room temperature LaB_6 emitter. This is an extraordinary large total current which would be difficult to sustain for any length of time in the case of a W emitter at room temperature. A few preliminary life tests have been performed on a heated ($T \cong 1500$ K) LaB_6 emitter. Life test runs at current levels of ~ 300 μA have been sustained for up to 60 hrs. In most instances the LaB_6 emitter did not undergo appreciable geometric change due to thermal-field build up.[21]

In summary, the LaB_6 Fe source has demonstrated that it can sustain large total currents at both room and elevated temperatures. Further work will be directed at establishing procedures to obtain reproducible emission distributions and to control the La/B ratio in the bulk as precisely as possible.

SECTION V

GAS PHASE FIELD IONIZATION STUDIES

Preliminary gas phase FI studies are being carried out with easy to handle gases such as H_2 and A. The principle aim of the studies reported here was to develop a gun that would provide a high intensity beam of ions using FI. Additional objectives of these initial studies are to determine emission characteristics such as beam noise spectrum, angular distribution and beam brightness.

A. Experimental Arrangement

Two FI sources were built for use on an optical bench and on a higher vacuum system. In each case the emitter was surrounded by a Mo cylinder (cathode cap) $\approx$ 1.5 cm in diameter with a thin aperture of 0.5 or 1.0 mm diam. at one end through which the ion beam was extracted. The aperture also served as a pumping port for the dynamic gas supply.[23]

H_2 was chosen as the gas for these experiments because it requires a field of $\approx$ 2.2 V/Å to ionize efficiently, which is similar to or higher than what is required for other gases such as Ar, N_2, O_2, or Xe.

The high vacuum study was performed in a glass field-ion microscope designed with an ion source shown in Fig. 19. The Mo cathode cap containing the beam aperture fits tightly around the glass LN_2 reservoir and is cooled by it. The configuration of the source was such that gas molecules made several collisions with the walls before escaping through the aperture, thus ensuring that the gas supply to the emitter would be at LN_2 temperature. Because the source configuration did not permit direct measurement of the gas pressure, measurements of the source geometry were made so that the pressure drop into the main chamber could

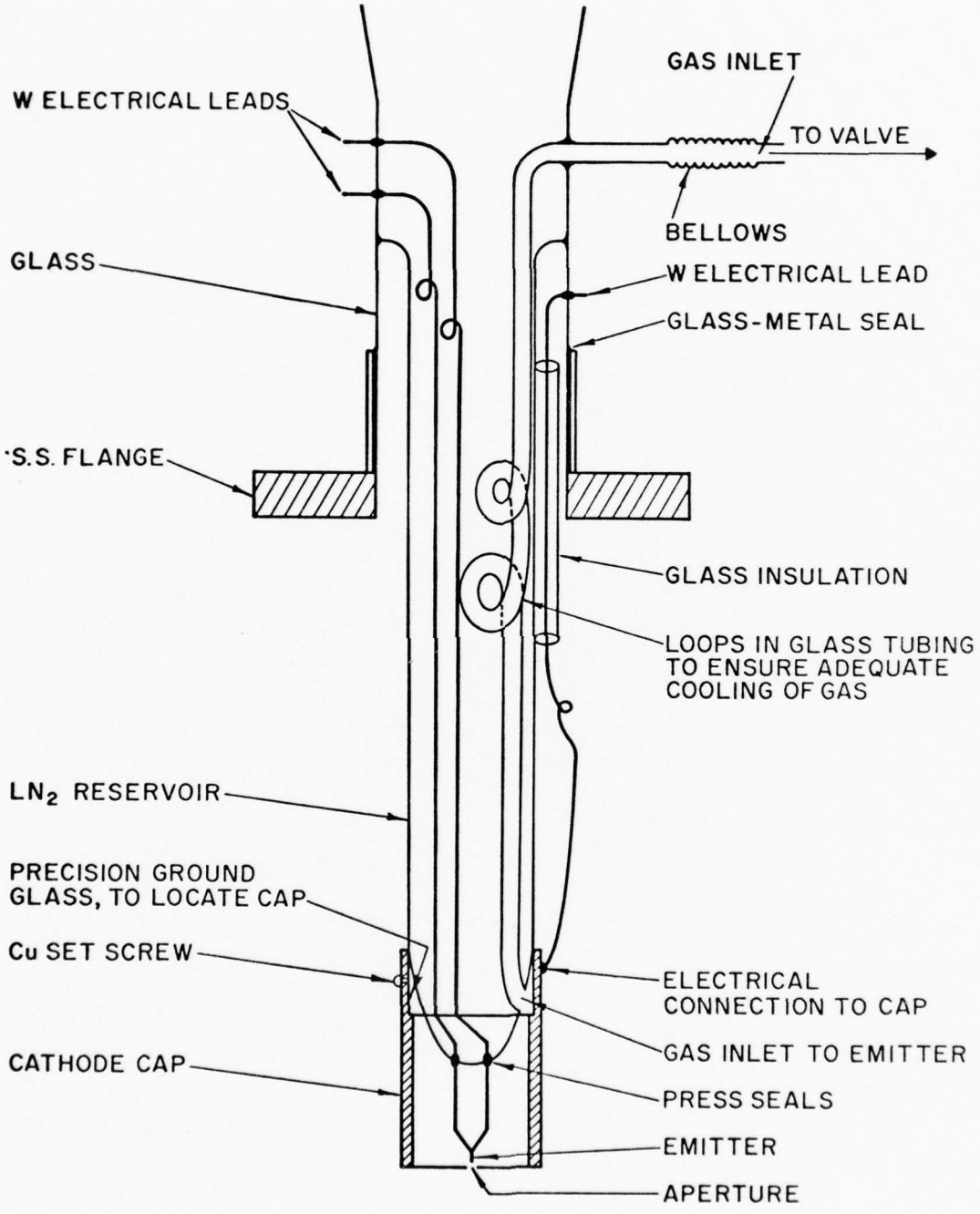

Figure 19. Diagram of a differentially pumped FI source. Filling the inner dewar with liquid N_2 cools the gas and emitter.

be calculated from kinetic theory. The pressure in the main chamber was monitored with an ionization gauge.

The ion beam was detected on a Willemite screen, where the intensity could be measured with either an electrometer connected to the screen or with a photomultiplier tube. The photomultiplier was interfaced to the screen with a light pipe which could be fitted with various apertures or lenses. H_2 was admitted into the source through a Pd "leak" via a finely controlled valve.

Current-voltage measurements were made with a Keithley 600A electrometer and a Sensitive Instrument Research Corporation electrostatic voltmeter. Voltages could be read to within 0.25% and were reproducible to that extent. The phosphor screen was biased at 22 V positive with respect to the grounded cathode cap to reduce the effects of secondary electrons. The whole source was shielded so that measurements of currents in the 10^{-12} A range could be made.

The optical bench system consisted of a metal casting, epoxy sealed, with numerous electrical, vacuum, and mechanical feedthroughs. The system utilized Viton "O" rings and was pumped with a 4-in. (10.2-cm) diffusion pump trapped with LN_2. A background pressure of $\sim 3 \times 10^{-5}$ torr was typical during the experiments. The optical bench allowed the insertion of a variety of electrostatic lenses, beam deflectors, apertures, targets, faraday cups, and a photomultiplier light pipe. The electron-optical components were held in "ways" machined to high tolerances so that all components were parallel and on axis.

The source used in the optical bench was similar in design to the one used in the high vacuum system, except that in the present form it

could not be cooled. Pressure in the source volume was measured with a General Electric thermistor pressure gauge fitted on the cathode cap. The gauge was calibrated with the system thermocouple gauge at 10^{-1} torr and with the system ion gauge at 10^{-3} torr.

Ion currents were measured with a faraday cup biased to prevent the escape of secondary electrons. For scanning work requiring a faster response than the electrometer, the beam was detected with a photomultiplier tube and a high speed scintillator.

Angular distributions were measured in the optical bench by using a four-plate deflection system, calibrated by deflecting an electron beam of known energy across two 100 μm apertures separated by 0.391 cm. The faraday cup was fitted with a slit aperture 1.2 x 12.5 mm located 40 mm from the emitter. The aperture subtended a solid angle of 9.4 msr and had a resolution of 30 mrad in the direction of deflection.

The emitters used in these experiments were made of Ir with radii generally 800-1500 Å, although emitters with radii down to 350 Å have been used. The emitters were examined and photographed with an electrostatic transmission electron microscope. Ir was chosen for the emitters because of its resistance to water etch and its general durability. Work done earlier in this laboratory has confirmed the superiority of Ir emitters to W emitters in any situation where water contamination might be present. A comparison of the properties of an Ir emitter and a W emitter after 0.3-h operation in an environment with $P_{H_2O} \sim 10^{-4}$ torr is shown in Figs. 20 and 21, where it may be seen that while the water had virtually no effect on the Ir, the W emitter performance was degraded by several orders of magnitude. A life test on an Ir emitter

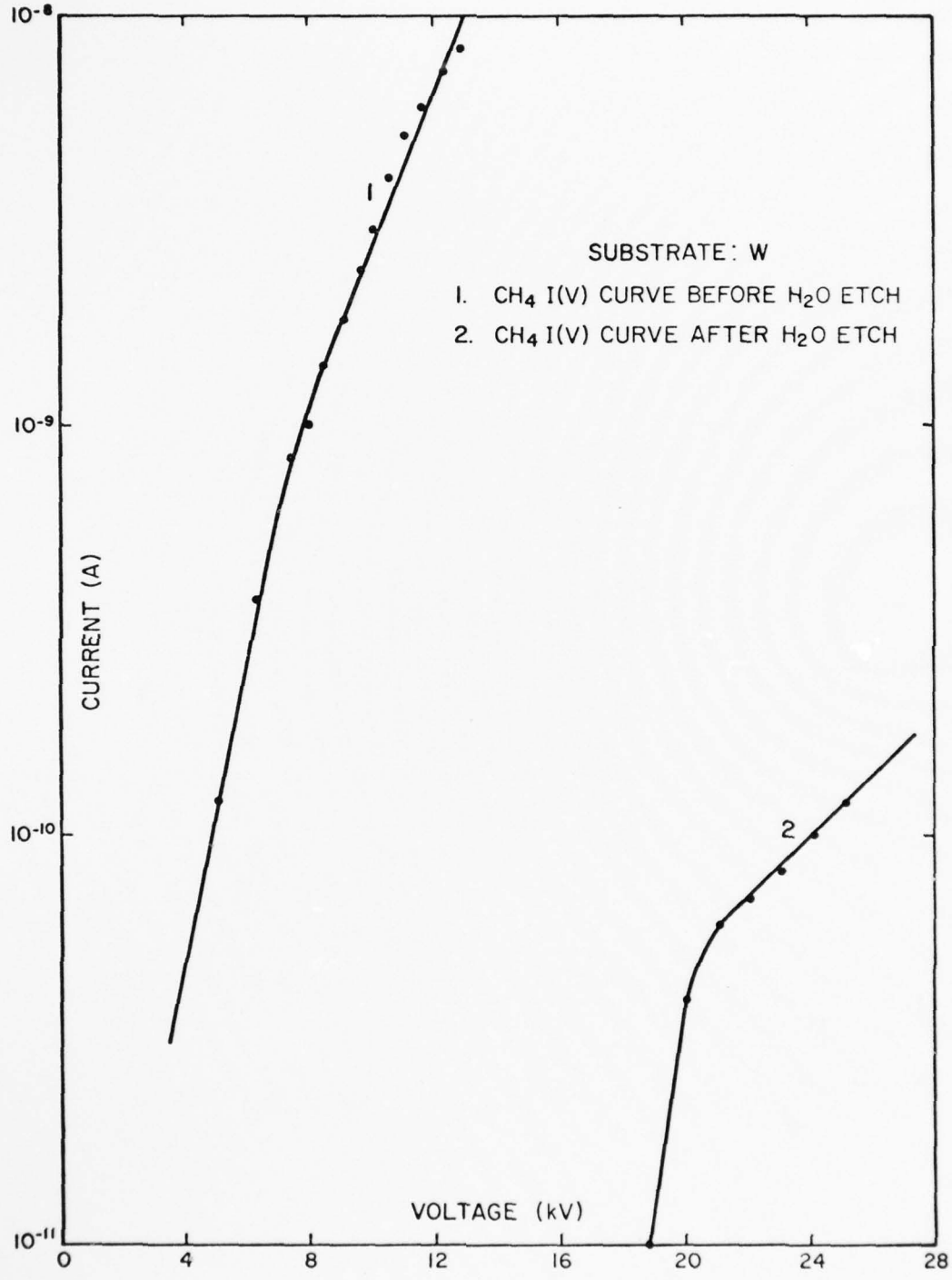

Figure 20. FI current vs voltage from a W emitter before and after 0.3-h exposure to H_2O at a pressure $P_{H_2O} = 10^{-4}$ torr.

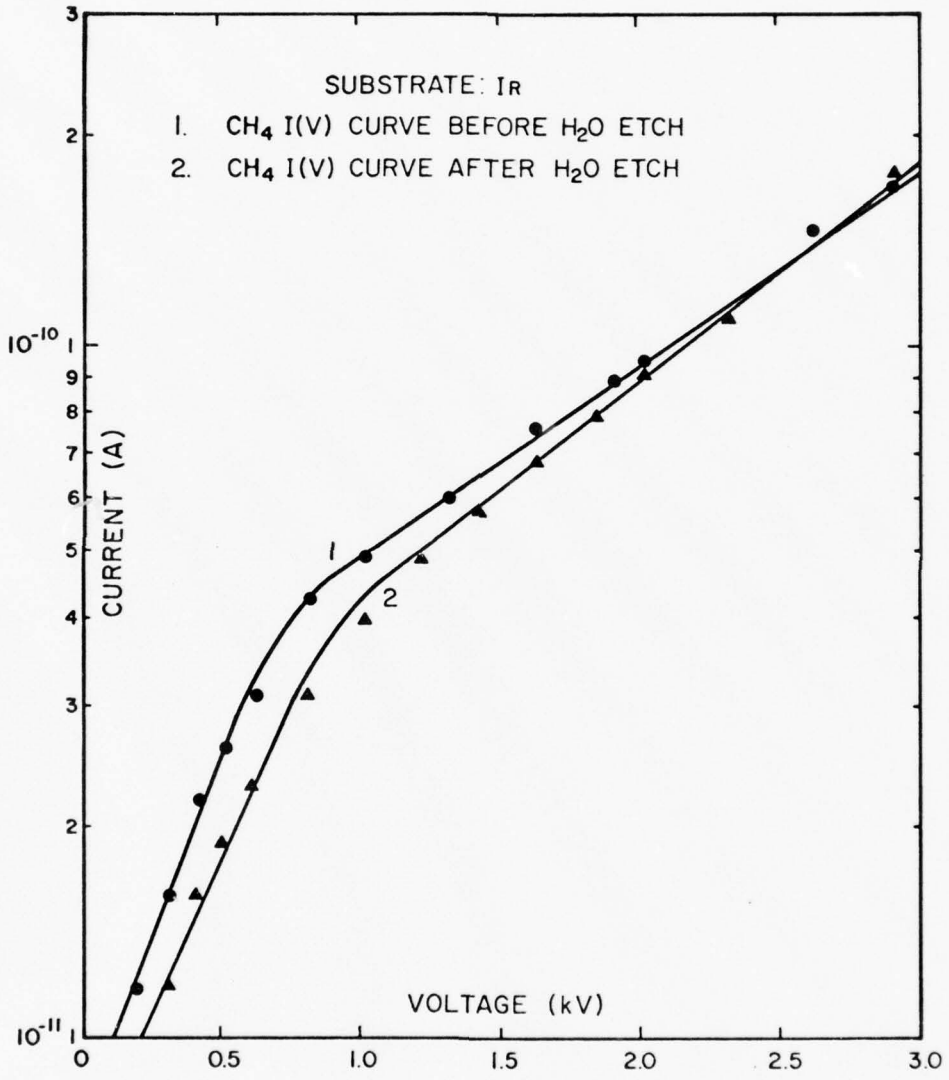

Figure 21. FI current vs voltage for an Ir emitter before and after 0.3-h exposure to H_2O at a pressure $P_{H_2O} = 10^{-4}$ torr.

at room temperature with $P_{H_2} = 10^{-3}$ torr showed no change in performance over a period of 12 h.

B. Results

1. Sensitivity

Ion current was measured as a function of H_2 pressure in both the optical bench and the high vacuum system to determine the sensitivity in A sr^{-1} $torr^{-1}$. Sensitivities were referenced at 3 kV above the best image voltage (BIV) or 3 kV above the break in the I-V curve as shown in Figs. 22 and 23. At room temperature (294 K) sensitivities of 0.5-3 x 10^{-6} A sr^{-1} $torr^{-1}$ were measured in the optical bench system. Sensitivities of 0.3 x 10^{-6} A sr^{-1} $torr^{-1}$ below 10^{-2} torr, rising to 0.7 x 10^{-6} A sr^{-1} $torr^{-1}$ at 3 x 10^{-2} torr were measured in the high vacuum system. The reason for the increase in sensitivity with pressure in the high vacuum system is not yet known. The greater sensitivity in the optical bench system may be due to low-ionization-potential contaminating gases entering the source with the H_2. At 77 K the sensitivity in the high vacuum system was measured to be 5 x 10^{-5} A sr^{-1} $torr^{-1}$ over the range 3 x 10^{-4} - 2 x 10^{-2} torr (see Fig. 24). These results are similar to work recently performed in this laboratory with an array of four Ir emitters where sensitivities of 6 x 10^{-6} and 3.7 x 10^{-5} A sr^{-1} $torr^{-1}$ were measured at 300 and 150 K, respectively.

When an emitter was placed 0.7 mm from the 0.5-mm aperture, the sensitivity was found to be about two times less than the first emitter which was 2.0 mm from the aperture. The latter result may be due to a lower emitter sensitivity, since no effort was made to ensure emitter uniformity by field desorption before use. On the other hand,

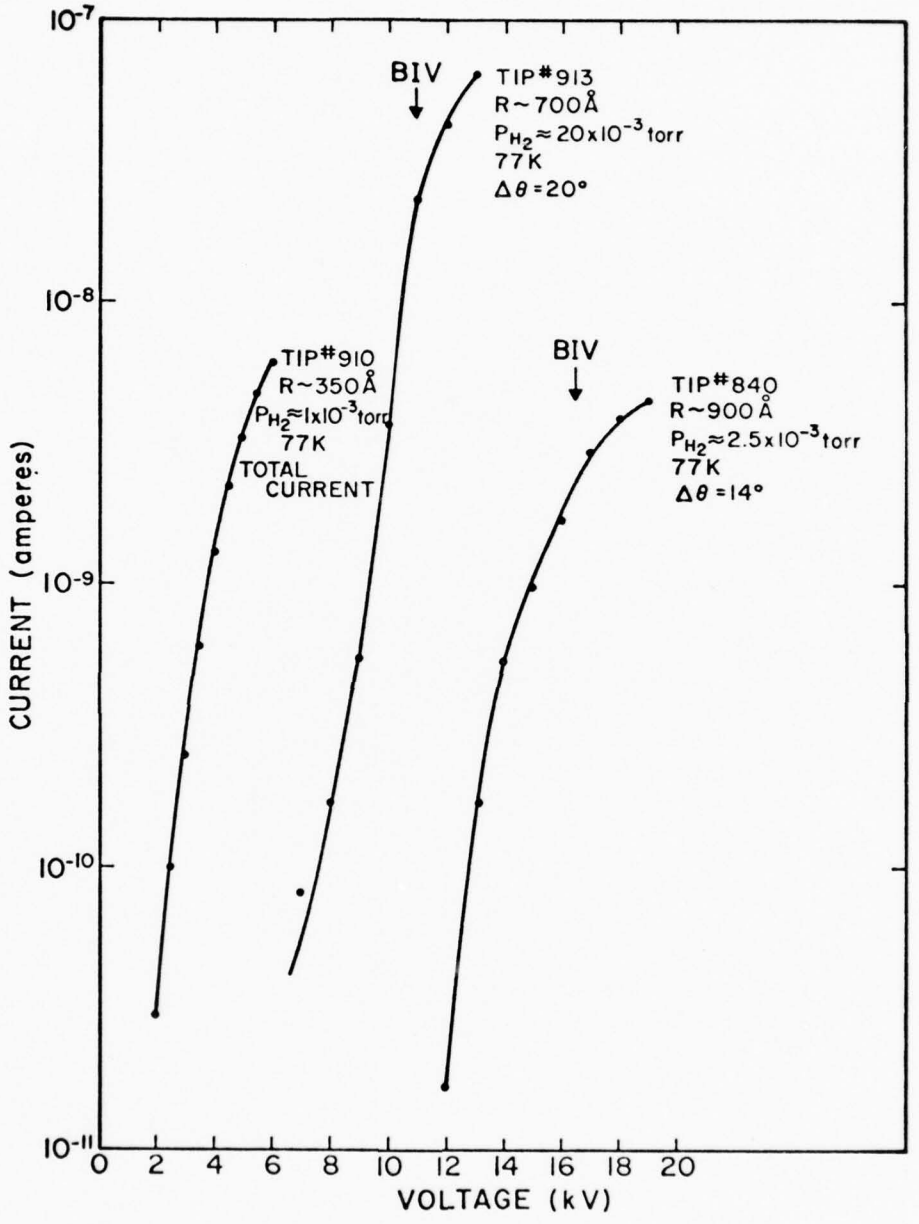

Figure 22. Current vs voltage measured for three emitters of varying radii and at various H_2 pressures in the high vacuum system. Current from emitters 840 and 913 was extracted through apertures with solid angles of 0.19 and 0.38 sr, respectively. Emitter temperatures were 77 K. BIV is the best image voltage and corresponds to ~ 2×10^8 V/cm.

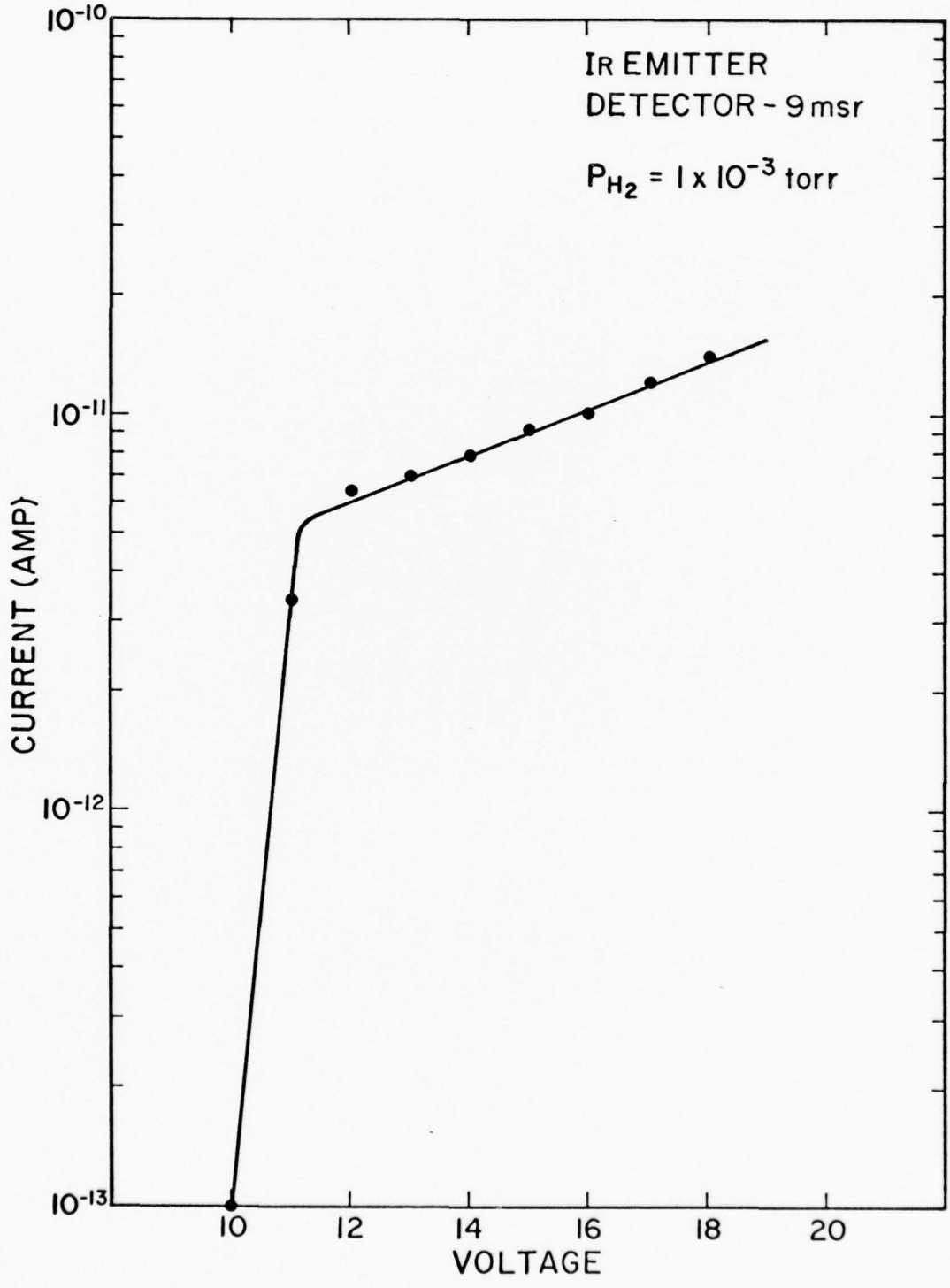

Figure 23. Current vs voltage measured for an emitter in the optical bench system at 294 K. The sensitivity was 1 x 10^{-6} A sr^{-1} $torr^{-1}$.

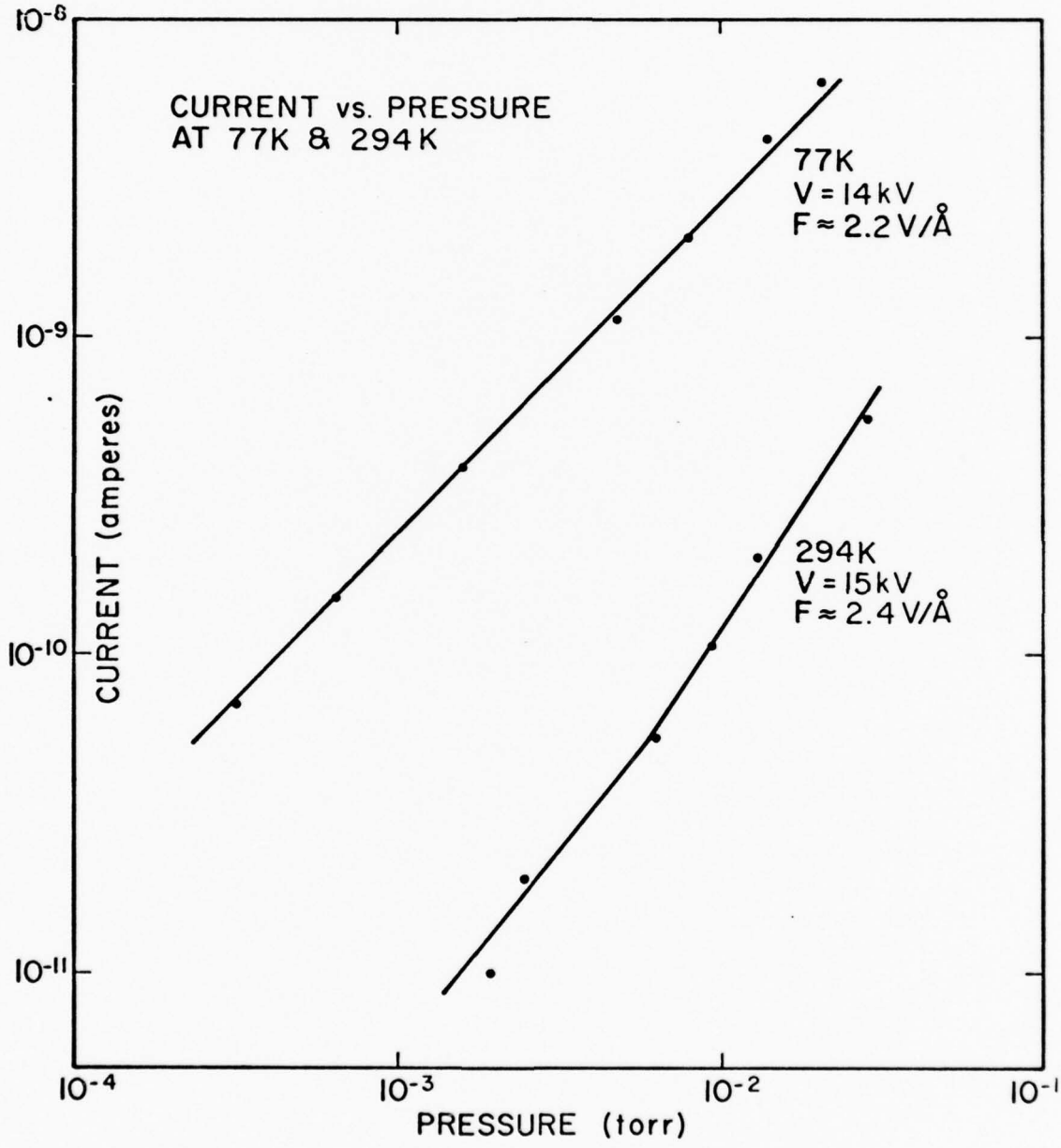

Figure 24. Current vs pressure for an emitter at 77 K and another at 294 K, showing the increased current available at low temperature.

the lower sensitivity may reflect a lower gas pressure near the aperture. It is to be expected that, at pressures corresponding to molecular flow, the pressure gradient through the aperture would manifest itself at a distance comparable to the aperture dimensions. The maximum H_2 pressure consistent with reasonable emitter lifetimes was $\sim 8 \times 10^{-2}$ torr at 294 K.

As mentioned previously, sensitivities were measured at field strengths of 2.3-2.6 V/Å - 10% to 20% above the BIV - in order to achieve maximum source current density within reasonable limits of beam energy spread. At these field strengths the ion current is roughly equally distributed between H^+ and H_2^+.[24] The bulk of the H^+ current falls within an energy spread of 2 eV and the bulk of the H_2^+ current within about 3 eV. The first Jason peak[25] for H_2^+ occurs about 7-10 eV below the main peak and is rather small in intensity. No Jason peak is seen for H^+.

2. Noise

The signal to noise ratio in the ion beam was measured with a spectrum analyzer attached to an EMI 9502B photomultiplier tube on the high vacuum system. The photomultiplier current I was monitored with a high quality microammeter. The background current I_{BG} and $(\Delta I_{BG}^2)^{1/2}$ were constant. The results are shown in Table IV. Since it was evident that there is relatively little noise in the signal above f = 10 Hz, the frequency of the spectrum analyzer was swept from f = 1-100 Hz with a bandwidth of Δf = 10 Hz with the beam on and then with the beam off. It was found that the spectral densities were practically identical above f = 15 Hz. It was noticed upon visual

TABLE IV

NOISE DATA FOR FI BEAM TAKEN WITH 10-HZ BANDWIDTH

f (Hz)	$I - I_{BG}$ μA	$(\Delta I^2)^{1/2} - (\Delta I_{BG}^2)^{1/2}$ μA	S/N
1	21	0.5	42
10	21	0.2	105
60	21	0.2	105
1	11	0.5	22
10	10	0.1	100
60	10	0.1	100

examination of the viewing screen that various emission sites on the emitter surface turned on and off in a random fashion, and it appeared that the main contribution to the low frequency noise is the current from these sites. Since the noise remained constant as the current was increased (by increasing the gas-supply pressure), it appears that the sites responsible for the noise emit independently of the gas pressure. Thus, as the current is increased the signal to noise ratio improves.

3. Angular Distributions

Angular distributions shown in Fig. 25 were measured with two emitters at 294 K in the optical bench system, with H_2 gas at 1×10^{-3} torr at 15 and 18 kV ($F \cong 2.6$ V/Å and $F \cong 2.3$ V/Å). The background pressure was 3×10^{-5} torr. The asymmetry of the angular distributions taken at right angles indicates a likely emitter orientation along the [111] direction.

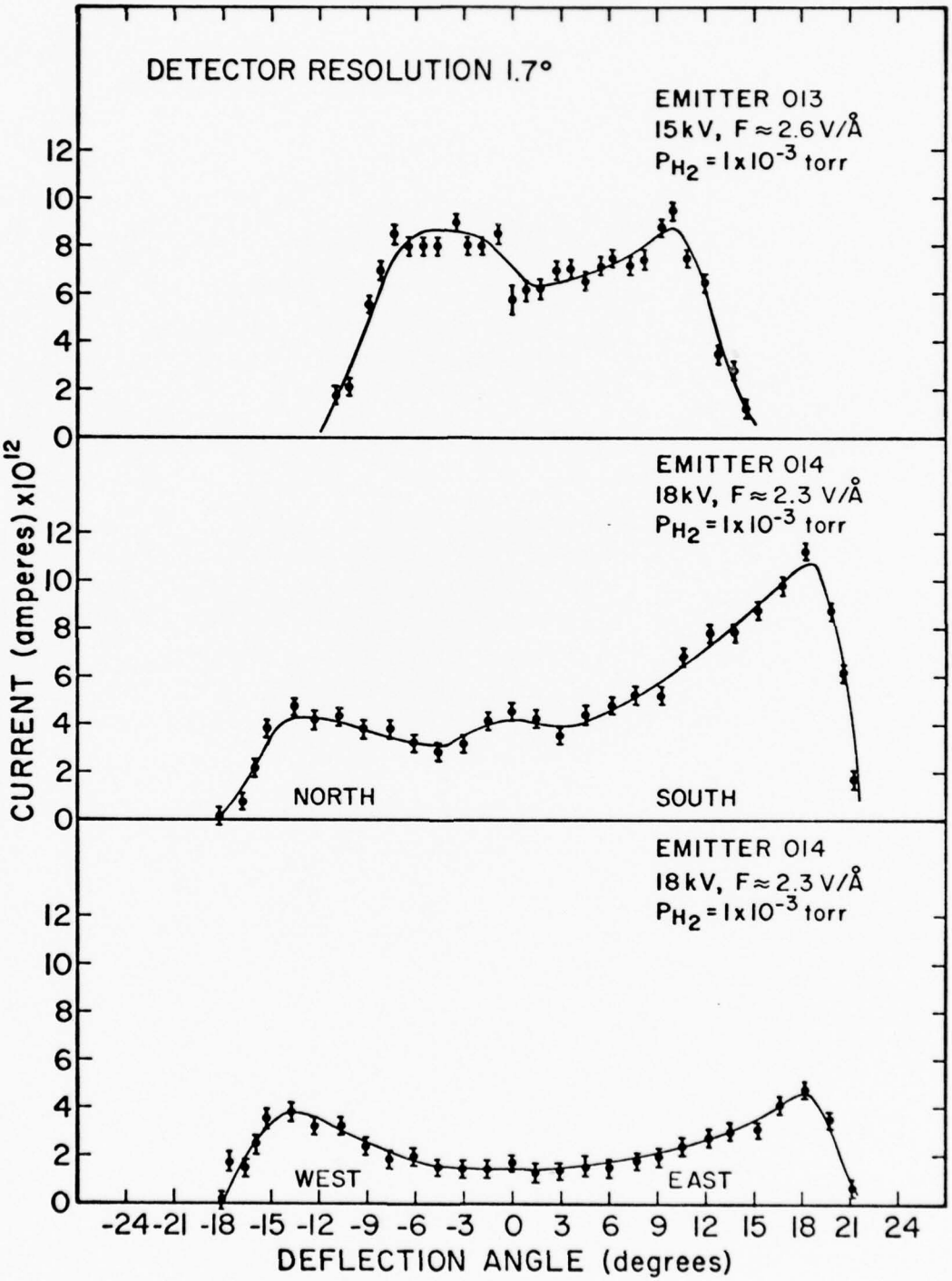

Figure 25. Angular distributions measured in the optical bench system at 294 K. The asymmetry of the orthogonal distribution indicates a likely emitter orientation along the [111] direction.

In Fig. 26 we show an angular distribution taken in the high vacuum system with a field of 2.3 V/Å at a H_2 pressure of 1.5×10^{-3} torr and an emitter temperature of 77 K. This was measured by slowly sweeping the photomultiplier, light pipe, and collimating aperture across the faceplate of the FI tube. The angular resolution is $\approx 3°$. The horizontal line represents the photomultiplier background current. These results show that the ion current is relatively uniformly distributed between $\pm$ 20°.

C. Summary

These preliminary results show that field ionization of gases can produce a low noise high brightness ion source suitable for microprobe applications. A simple source has been designed which allows the high gas pressure to be confined to the emitter region of the ion gun. Cooling the incoming gas and emitter increases the ion current to a value of 5×10^{-5} A sr^{-1} $torr^{-1}$.

According to the Fig. 5 results an aperture half angle of 12 mrad gives a virtual source size of 10 Å for $F = 2 \times 10^8$ V/cm, V = 19 kV, and ρ_{oo} = 1000 Å. This value of virtual source size coupled with the above mentioned angular intensity for H_2 yields a source brightness of $\sim 2 \times 10^7$ A sr^{-1} cm^{-2} for a gas pressure of 1×10^{-2} torr. A duoplasmatron ion source developed by Drummond and Long[26] has a brightness of 400 to 1000 A sr^{-1} cm^{-2} at 20 kV, which represents the state of the art for conventional cathodes.

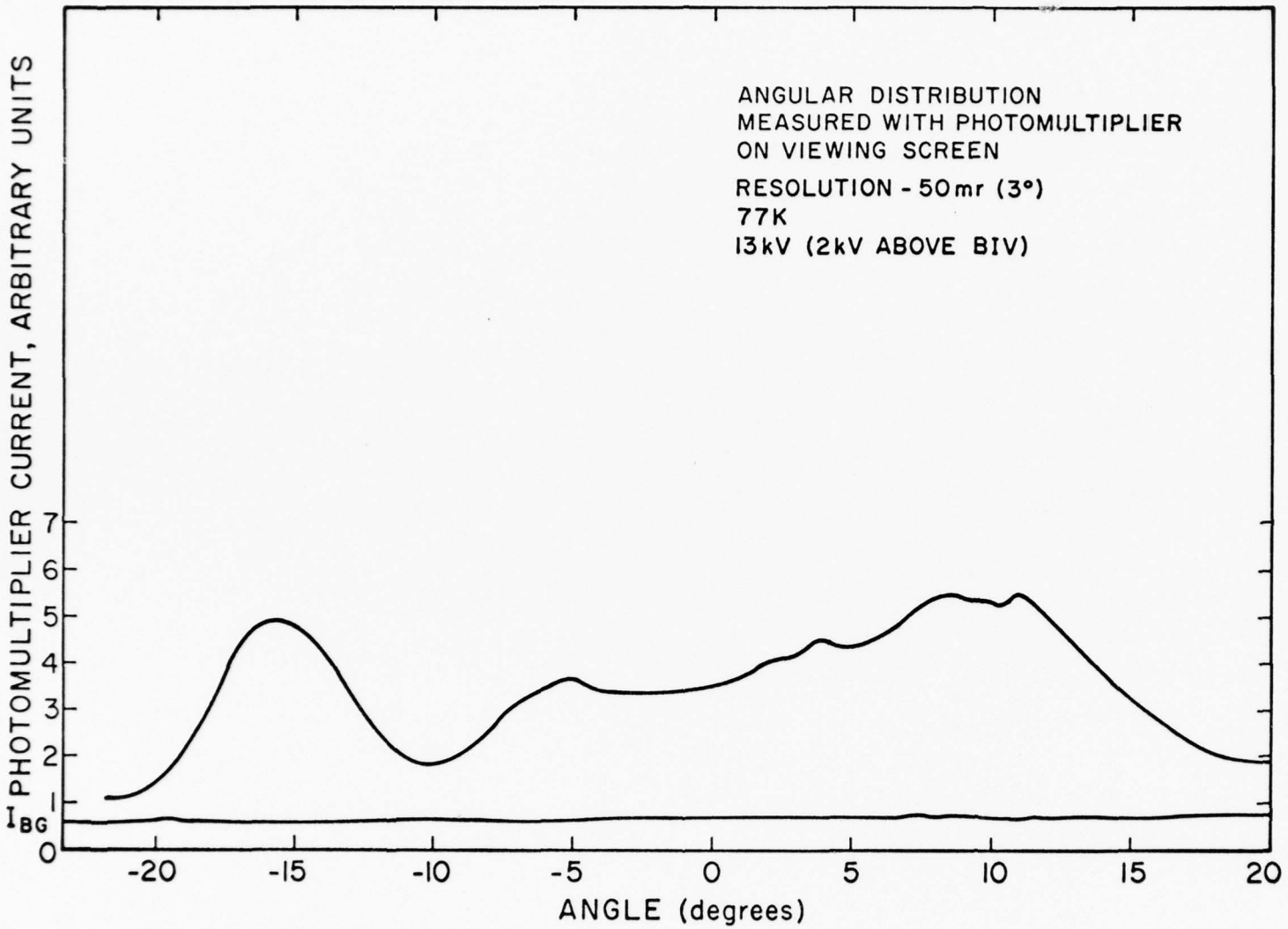

Figure 26. Angular distribution measured in the high vacuum system with a photomultiplier. The photomultiplier light pipe was apertured to accept only 3° of the beam measured at the emitter. I_{BG} represents the background in the photomultiplier.

SECTION VI

LIQUID GALLIUM FIELD EMISSION STUDIES

A new type of field emission source suitable for both electron and ion emission is a pointed emitter of liquid Ga. The liquid field emission source is frequently referred to in the literature as an electrohydrodynamic (EHD) source because of its method of operation. Its history goes back to the early days of electric propulsion research when various fluids were being used to form charge droplets by spraying from small nozzles with high electrostatic fields.

The method consists of exposing a conductive liquid-metal-vacuum interface to a high electrostatic field produced near the tip of a small capillary tube (typically between .02 and .08 mm radii). The interaction of the electrostatic stresses with surface forces of the liquid results in the formation of a liquid cone extending outward from the capillary tip. Near the liquid cone apex, the fields are sufficiently high ($> 10^7$ V/cm) to extract ions by field evaporation or, if the field polarity is reversed, electrons by field electron emission.

The production of charged particles from Wood's metal,[27] Ga and Sn,[28] Cs[29] and a Ga-In alloy has been investigated.[30-31] In the case of the Ga-In eutectic alloy the major ions produced are Ga^+ and In^+ with a wide variety of multiply charged molecular ions.[31]

A. Theory of Operation

It is hypothesized that ion emission from a liquid metal surface originates near the apex of a single conical jet where the field is sufficiently large to field evaporate ions. Formation of conical

geometries when a liquid surface is exposed to a high electric field has been demonstrated experimentally.[30,33] The problem of determining the allowed equilibrium shape of a liquid surface so that the electrostatic stress f_e normal to the surface is exactly balanced by the surface tension f_s forces was treated by Taylor.[33] The surface tension force is given by

$$f_s = \gamma_s \left(\frac{1}{\rho_1} + \frac{1}{\rho_2} \right) \tag{21}$$

where γ_s is the surface tension and ρ_1 and ρ_2 are the principle radii of curvature. For a sphere, cone, and infinitely long cylinder Eq.(21) becomes respectively

$$f_s \text{ (sphere)} = 2\gamma_s/\rho \tag{22}$$

$$f_s \text{ (cone)} = \frac{\gamma_s \cot\alpha}{R} \tag{23}$$

$$f_s \text{ (cylinder)} = \gamma_s/\rho \tag{24}$$

where ρ is the respective radii and α is the cone half angle and R the distance along the cone axis. Since the electrostatic stress is given by

$$f_e = \frac{F^2}{8\pi} \text{ (dynes/cm}^2\text{)} \tag{25}$$

the conditions for equilibrium between the external electrostatic and internal surface tension forces are

$$F \text{ (sphere)} = 4 \left(\frac{\pi\gamma_s}{\rho} \right)^{1/2} \tag{26}$$

$$F \text{ (cylinder)} = \left(\frac{8\pi\gamma_s}{\rho} \right)^{1/2} \tag{27}$$

$$F \text{ (cone)} = \left(\frac{8\pi\gamma_s \cot\alpha}{R} \right)^{1/2} \tag{28}$$

If an anode is a distance a from the surface of the sphere or cylinder, the voltages required for the above conditions are

$$V \text{ (sphere)} = \rho^{1/2}\, 4(\pi\gamma_s)^{1/2}\left(1 - \frac{\rho}{a}\right) \tag{29}$$

$$= 2.13 \times 10^3\, \gamma_s^{1/2}\rho^{1/2}\left(1 - \frac{\rho}{a}\right)$$

$$V \text{ (cylinder)} = \rho^{1/2}\, (8\pi\gamma_s)^{1/2}\, \ell n\, \frac{\rho}{a} \tag{30}$$

$$= 1.5 \times 10^3\, \gamma_s^{1/2}\, \rho^{1/2}\, \ell n\, \frac{\rho}{a}$$

where V is in volts, γ_s in dynes/cm and ρ in cm. For the case of a cone the angle α must be found so that $F \propto R^{-1/2}$. Taylor[33] showed that this would occur only if $\alpha = 49.3°$, in which case Eq.(28) becomes

$$F \text{ (cone)} = .93\left(\frac{8\pi\gamma_s}{R}\right)^{1/2} \text{ (V/cm)} \tag{31}$$

and the potential of an anode surface a distance R from the cone apex is given by

$$V \text{ (cone)} = 1.4 \times 10^3 \gamma_s^{1/2}\, R^{1/2} \tag{32}$$

Most experimental studies have confirmed that the cone formed by the electrostatic forces has a cone half angle $\alpha \cong 49°$ as predicted. However, in many cases a small cylindrical column extends out from the cone apex. A comparison between Eqs.(27) and (31) shows that the field required to stabilize a cylinder of radius ρ and a cone truncated at $R = \rho$ is approximately the same.

In some instances small charged droplets are emitted from the end of the cone. Mahoney, et al[29] concluded that ion, as opposed to droplet, formation will occur if the tensile strength f_t of the liquid is large compared to the electrostatic stress required for field evaporation, i.e. f_t/f_e is large.

An approximate expression for the field required for field evaporation from metals is

$$F_{FE} = e^{-3} \left(H_{VAP} + I - \phi - kT \ln \frac{\tau}{\tau_o} \right)^2 \qquad (33)$$

or

$$F_{FE} = .069 \left(H_{VAP} + I - \phi - kT \ln \frac{\tau}{\tau_o} \right)^2 \ (V/\mathring{A}) \qquad (34)$$

where H_{VAP} is the heat of vaporization I, the ionization potential, τ, the life time with respect to field evaporation and $\tau_o \cong 10^{-12}$ sec. The second expression is correct for H_{VAP}, I, kT and ϕ in eV and F in $V/\mathring{A}$. The value of τ can be arbitrarily chosen as 1 sec. It should be pointed out that the above expressions assume singly charged ionic species being evaporated. Table V lists the values of F_{FE} at 300K and other relevant parameters for several liquid metals.

TABLE V

EVAPORATION FIELDS FOR ION EMISSION FROM LIQUIDS

Element	Vaporization Energy H_{VAP} (eV)	Ionization Potential I (eV)	Work Function ϕ (eV)	Surface Tension (dyn/cm)	Evaporation Field F_{FE} $(V/\mathring{A})$
Cs	0.81	3.87	1.81	60	.36
Rb	0.85	4.16	2.09	76	.32
K	0.93	4.32	2.24	86	.40
Ga	2.82	5.97	4.12	735	1.14
Hg	0.64	10.39	4.53	480	2.44

The theoretical tensile strength of the liquid column can be estimated by

$$f_t = 2\gamma/r_o \ .$$

where r_o is the interatomic spacing. Mahoney, et al,[29] have tabulated values of r_o, f_t and f_c which are reproduced in Table VI.

TABLE VI

RATIO OF SURFACE ELECTROSTATIC STRESS AT ION EVAPORATION FIELDS TO THEORETICAL STRESS NECESSARY TO RUPTURE A LIQUID COLUMN

Element	Interatomic Distance r_o (Å)	Tensile Strength $f_t \times 10^{-10}$ (dyn/cm^2)	Electrostatic Stress $f_e \times 10^{-10}$ (dyn/cm^2)	Force Ratio f_t/f_e
Cs	5.31	0.226	0.0545	4.16
Rb	4.97	0.317	0.0428	7.1
K	4.70	0.365	0.069	5.2
Ga	2.77	5.3	0.562	9.4
Hg	3.07	3.14	2.57	1.2

According to Table VI Ga should be one of the most favorable liquids for field evaporation of ions because of the large ratio of f_t/f_e. A further important property possessed by liquid Ga is its low vapor pressure or alternatively its high value of H_{vap}. At room temperature its vapor pressure is completely negligible and at 825 K its vapor pressure is only 10^{-8} torr. This means that negligible gas phase electron impact ionization of Ga occurs during electron emission and that negligible gas phase field ionization occurs during ion emission. In the case of the source configuration shown in Fig. 28(c) the Ga supplies the emitter via surface diffusion. If the Ga wets the emitter surface then supply to the emitter tip occurs by self surface diffusion of Ga. An important factor is the mean distance $\bar{X}$ the Ga can diffuse before evaporation occurs, since this will limit the supply of Ga to the emitter. It can be shown that $\bar{X}$

is approximately given by

$$\bar{X} \cong a_o \exp (H_{vap} - E_{diff})/2kT \qquad (35)$$

where E_{diff} is the activation energy for self diffusion and a_o is the mean jump length for the diffusing particle. In view of the large value of H_{vap} for Ga, it is clear from Eq.(35) that $\bar{X}$ is very large at room temperature. According to this model it would be profitable to increase the source temperature, in order to increase the diffusion rate, until the value of $\bar{X}$ is approximately equal to the distance between the emitter tip and the Ga reservoir.

According to Eq.(32) the anode voltage required to stabilize the liquid cone depends only on γ_s and R. For Ga, Cs, and Hg the required anode voltages for R = 1 mm are 12.35, 3.5 and 9.9 kV respectively.

B. Experimental

Figure 27 gives a cross-sectional representation of the apparatus used for liquid field emission studies. The extractor and screen can be either positive or negative high voltage enabling both electron and ion field emission to be studied. The rubber diaphragm allows the vessel to be evacuated before inserting the liquid through a hyperdermic syringe; thus preventing any oxidation of the liquid metal. Once inserted, the position of the liquid metal meniscus is controlled by adjusting the gas pressure via two air valves, one leading to an argon pressure source, the other to a mechanical pump. The pressure inside the main vessel is maintained at $\approx 10^{-7}$ torr.

The two needle configurations that have been used are shown in Fig. 28. The tips are so shaped to aide the liquid metal in wetting the needle. Because of rapid attack by the liquid Ga the Pt nozzle was discarded. The work reported here was carried out with the W nozzle shown in Fig. 28(b). Presently studies are being carried out with a W emitter insert shown in Fig. 28(c). The latter design operates at a lower voltage (depending on the emitter length) and supplies Ga to the end of the emitter through a surface film of Ga wetting the emitter. A small field stabilized cone appears to form on the end of emitter thus localizing and stabilizing the geometric location of the virtual source.

The liquid metal being used was a Ga/In alloy, containing a eutectic mixture of 12% wt. In. This mixture was chosen because of its relative high wetting coefficient, and low melting point (18°C), thus eliminating any need for heating during the experiment.

Fig. 29 shows the simple circuit employed to measure the field emission. R is a current limiting resistor and the attenuator reduces

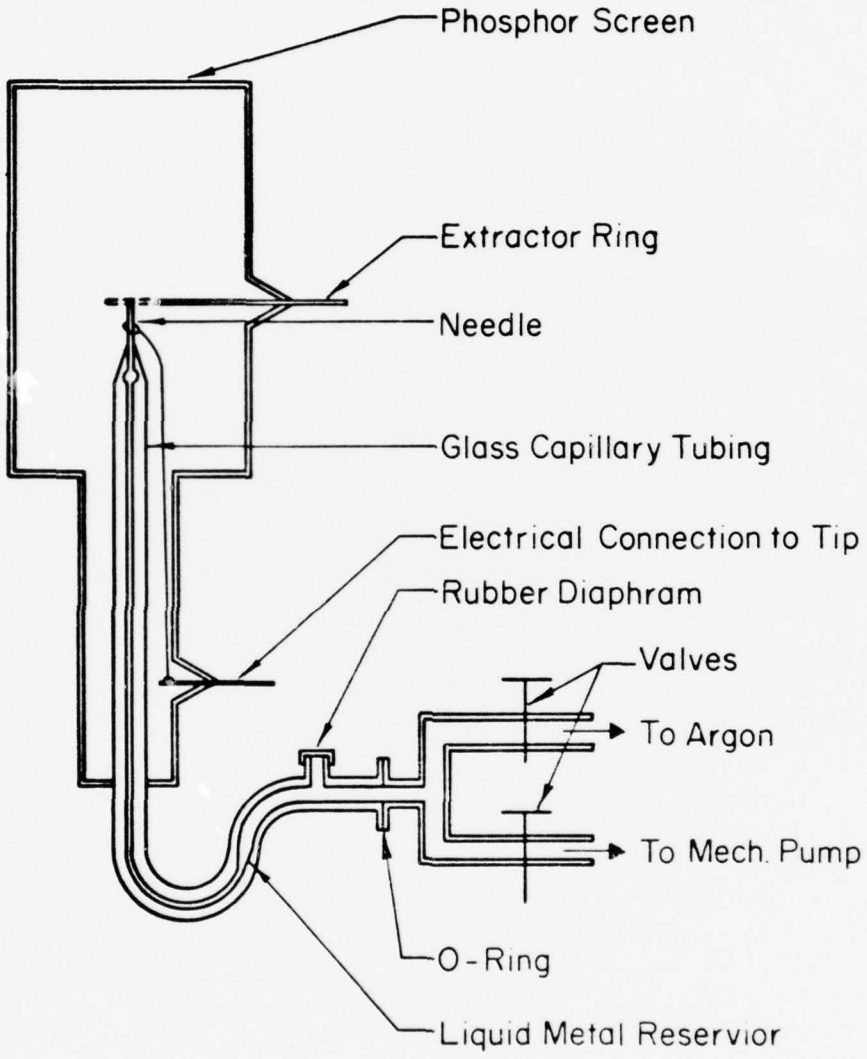

Figure 27. Diagram of the liquid Ga source and tube used to study electrons and ion emission.

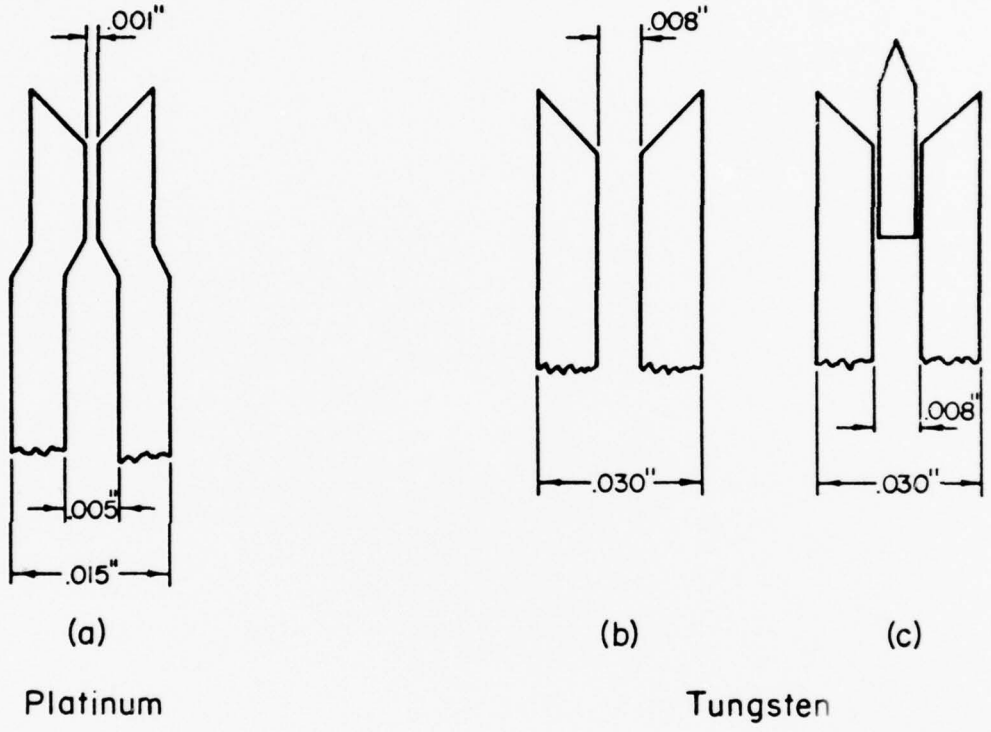

Figure 28. Diagram of the platinum (a) and tungsten (b) and (c) sources employed to study electron and ion emission from liquid Ga. Liquid Ga was fed to the nozzle by a positive pressure differential.

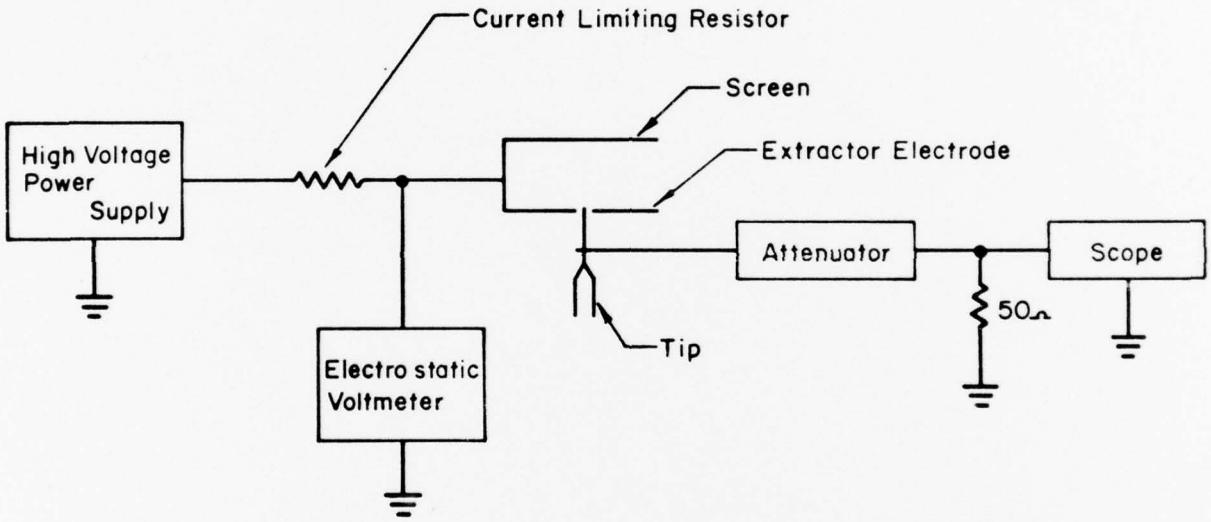

Figure 29. Diagram of the electrical circuit employed in the liquid Ga studies.

the signal to a magnitude the scope can measure. The general experimental procedure was to evacuate the vessel, insert liquid metal via the septum, force the liquid metal into the needle tip, and apply high voltage of the desired polarity. It was found that the ability of the liquid metal to wet the needle was greatly enhanced by sputting it with argon for several minutes. Without sufficient wetting, the electrostatic forces would pull the liquid metal off of the tip before a voltage high enough to create emission could be reached.

1. Experimental Results

Emission in both the electron and ion modes was initiated by advancing liquid metal to the nozzle end and then applying the high voltage. Emission usually began between 9.5 and 10.5 kV and was always accompanied by a localized blue glow. If the proper amount of liquid metal was at the nozzle end the liquid metal would form an upright cone approaching Taylor's theoretical half angle of 49.3°. Fig. 30 shows a photograph of the nozzle and liquid Ga cone formed during electron emission. When the cone forms, emission is very stable throughout the voltage range (9 to 20 kV). If too little liquid metal was at the nozzle end, then emission occurred from small cones formed on the edge of the nozzle. The cone provided a steady current if the voltage remained constant, but moved spatially and often formed multiple emission points as the voltage was increased. Excess liquid metal on the tip caused an unstable upright cone to form that was in continuous motion and provided very unstable emission.

Once an upright stable cone was formed emission became very stable. The threshold emission voltage remained constant, and the

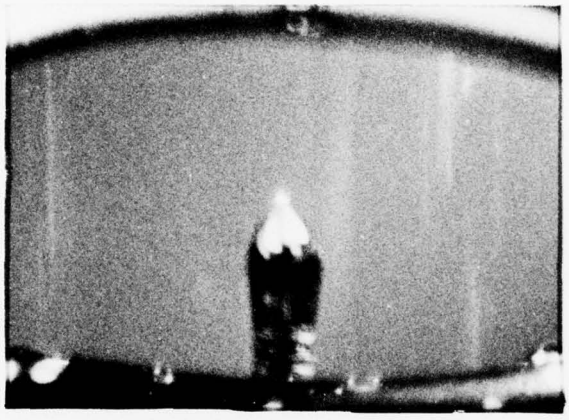

Figure 30. Photograph of liquid Ga cone formed on the tungsten nozzle shown in Fig. 28(b).

cone could be made to collapse and reform repeatedly by varying the voltage across the initial threshold voltage. It was possible to leave the system off overnight and to turn the system on in the morning and to measure the same emission characteristics as measured prior to turning the system off. For a given cone, the initial emission voltage was very sharply defined.

2. Electron Emission

Thus far electron emission has exhibited only one mode of operation - the pulse mode. This mode is characterized by high current, short duration pulses which occur at a constant rate producing average currents of 1 μa to 2.5 mA. The pulse form remains constant in shape, magnitude and duration, while the pulse rate changes with voltage and the current limiting resistor. Thus changes in the average current are due to the pulse rate and not the pulse. A typical pulse, as shown in Fig. 31(a), is 90-120 Amperes, 10 nanoseconds duration, and gaussian in shape. The pulse frequency remains very stable and can be made to vary from 55 Hz to 2 kHz. The pulse frequency is stable and can be increased or decreased by changing either of the two variables which effect it, the voltage or the current limiting resistor. Fig. 31(b) shows the voltage trace at the extractor electrode of the tube. The sharp drop in extractor voltage was due to the Ga discharge shown in Fig. 31(a) which was followed by a charging rate governed by the tube capacitance and load resistor. As shown in Figs. 32 and 33 the pulse rate increases with increasing voltage or decreasing load resistance.

The voltage at the extractor electrode shown in Fig. 31(b) exhibits a pattern similar to an R-C circuit. The period of the pattern

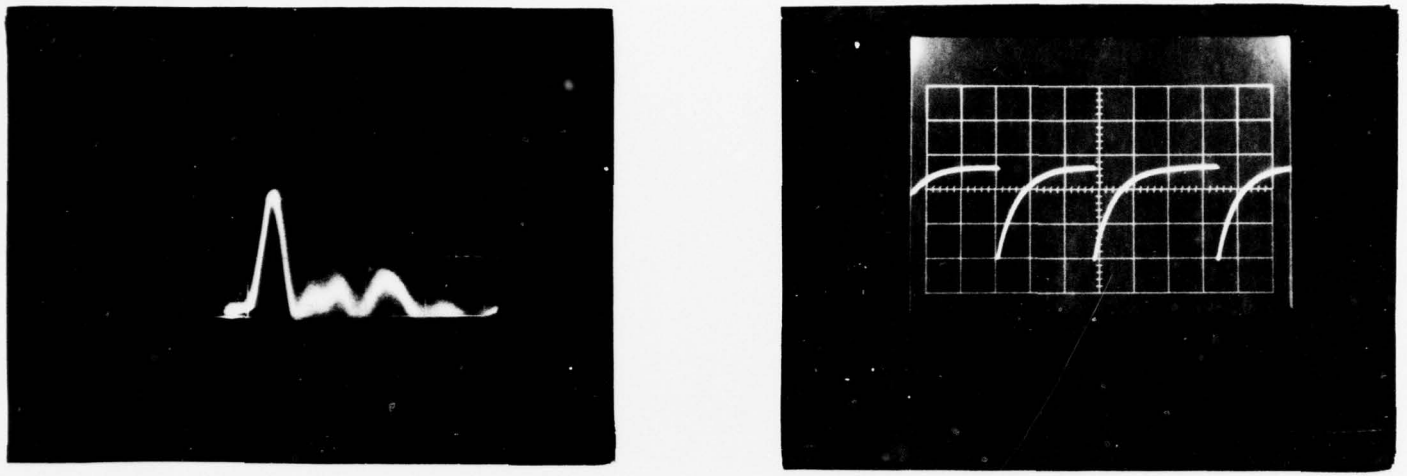

(a) (b)

Fig. 31. Photo (a) shows pulsed electron emission oscilloscope trace from liquid Ga: load resistor 30 MΩ, V = 14 kV, 10 nsec/div, peak current ~ 100 A. Photo (b) shows the voltage trace of the RC charge up on the tube anode; the time base is 2 msec/div and amplitude is 5 kV/div.

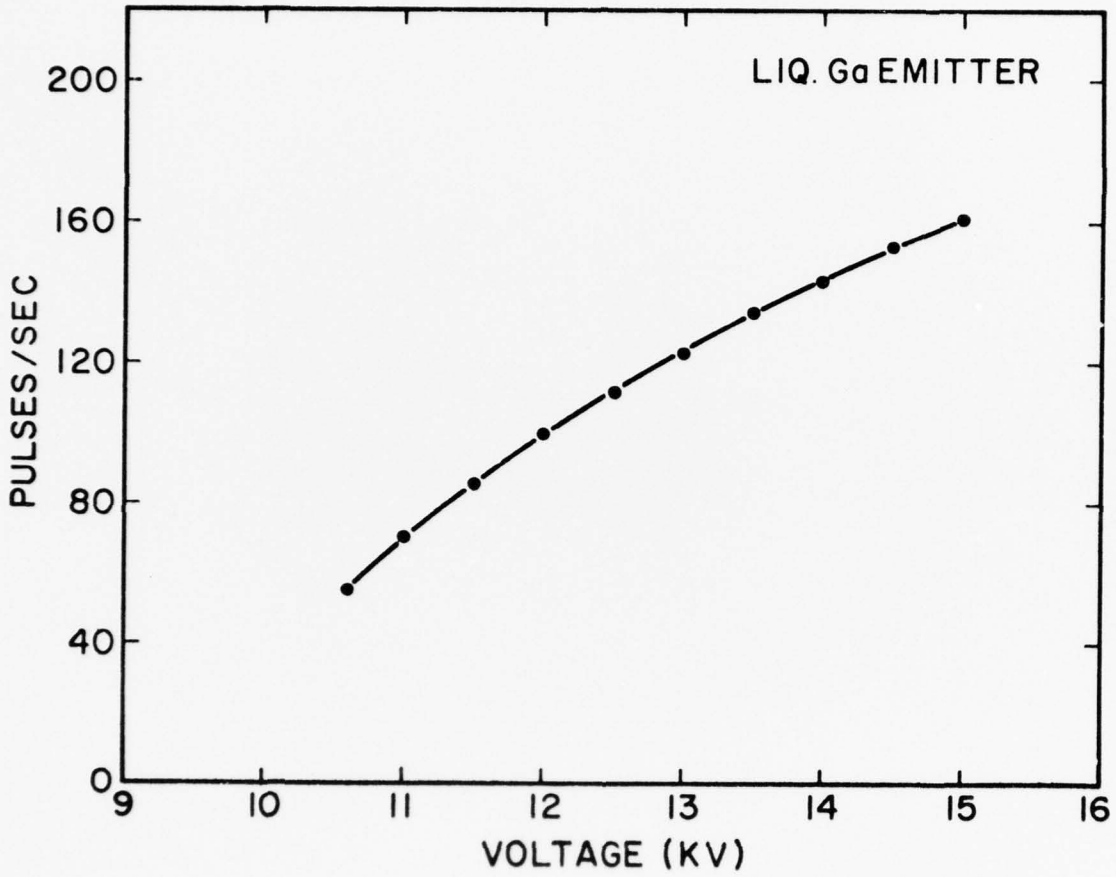

Figure 32. Plot of pulse rate vs anode voltage for electron emission from liquid Ga using a load resistor of 500 mΩ.

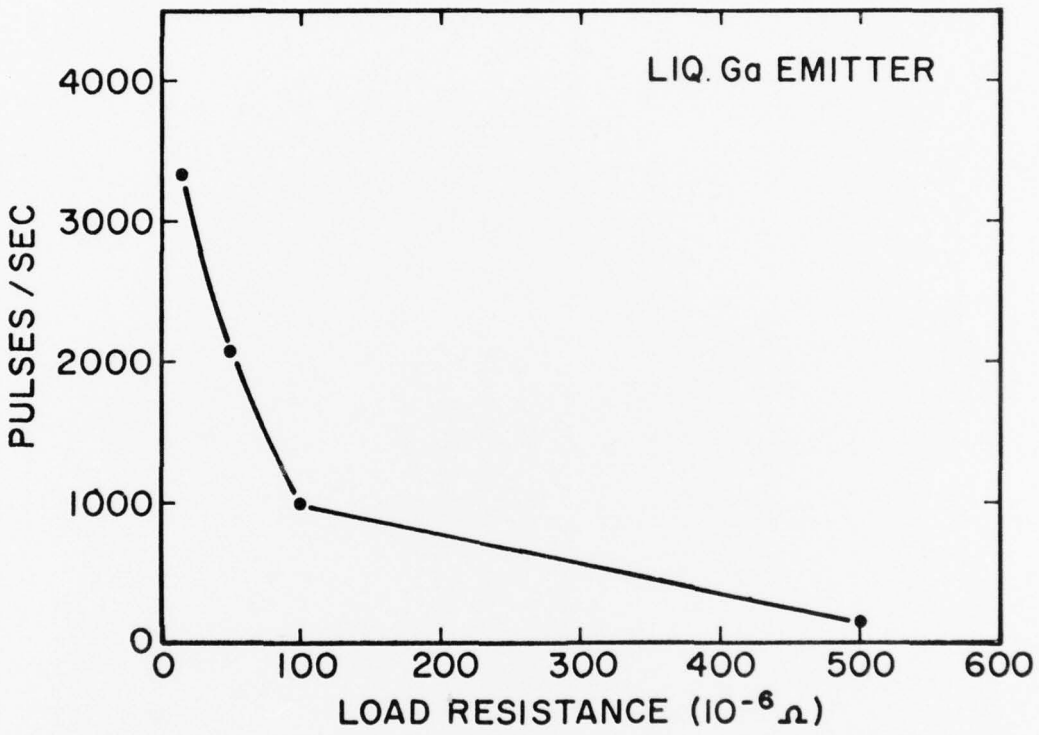

Figure 33. Plot of the pulse rate of electron emission from liquid Ga vs load resistance for an anode voltage of 12 kV.

equals the period of the pulses. This indicates that the tube was acting as a capacitor, storing up charge and then discharging during the pulse. Thus, increasing the voltage or decreasing the current limiting resistance allowed the apparatus to charge more rapidly and thus increase the pulse rate. By considering the system as an R-C circuit with the glass tube as a capacitor then the time, t, to charge the capacitor is

$$t = -RC \ln\left(\frac{V_o - V}{V_o}\right) \tag{36}$$

where R is the load resistor and C is the tube capacitance. Using t as the pulse rate, an average current vs voltage curve was obtained and, as shown in Fig. 34, partial agreement with the measured average current was obtained. The upward deviation of the measured average current was believed to be due to an additional emitting site formed at that voltage. A tube capacitance of 8 pf was calculated.

The maximum average current measured was 3.5 mA at 12 kV and 1.1 mΩ current limiting resistance. This current was sufficient to heat the extractor electrode to red glow. Therefore higher pulse frequencies were not attempted, but there is no reason to believe they are not possible. These studies were carried out in a vacuum of 1 to 5×10^{-7} torr although in one case air was leaked into the tube to 1×10^{-4} torr with no deleterious effect on the electron emission.

3. Ion Emission

Ion emission exhibited three modes of operation, a d.c. mode, pulse mode, and high frequency mode. The pulse mode has the same characteristics as the electron pulse mode with the following differences: the pulse is smaller, about 2.2 mA, and the pulse rate is constant only to a factor ± .1 msec. This slight inconsistency of the rate means

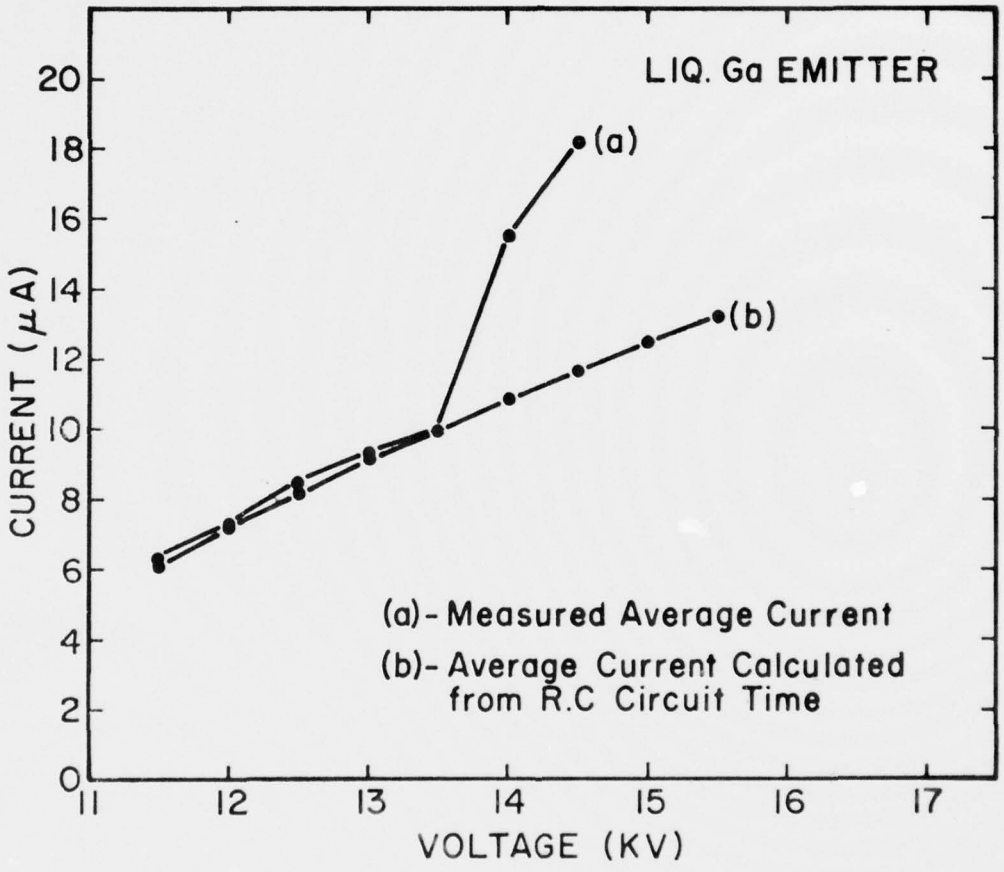

Figure 34. Plot of the measured average (a) and calculated average (b) electron current (using Eq.36) from liquid Ga vs anode voltage using a 500 mΩ load resistor.

nonconstant triggering of the scope which prohibits the viewing of a single pulse. Average currents of 1 μA to .5 mA were obtained during the pulse mode.

The d.c. mode was obtained within a narrow range of current limiting resistances and was very sensitive to change in voltage. A voltage change usually resulted in the high frequency mode while larger voltage changes resulted in the pulse mode. The d.c. mode could not be maintained for periods longer than a minute. This mode occurred from 9.8 kV to 11.5 kV producing a constant current of 70 to 140 μA.

The high frequency mode appeared when a small voltage change took place during the d.c. mode operation. This mode exhibited a nonuniform high frequency signal. Generally the d.c. mode degenerated into the high frequency mode with time or voltage change.

The important feature of the ion emission appeared to be the value of the current limiting resistance. The d.c. and high frequency modes were seen only with a 10 mΩ limiting resistance. The key to obtaining d.c. mode with either electron or ion emission seems to be in the external circuit and nozzle geometry. More recent experiments with the emitter configuration shown in Fig. 28(c) are now giving more stable d.c. ion emission over a wide range of load resistance.

C. Discussion of Results and Conclusions

In both the electron and ion modes of operation a small point source of blue light emanates from the tip of the Ga cone. This is an indication that electronic excitation of the Ga occurs during the emission process.

From the fact that only a pulsed mode of operation has been observed with electron emission it appears that the electrostatic forces cause the liquid cone apex to approach an infinitely small point. This, in turn, leads to an increasing field and, hence, emitted current. Accordingly the cone is heated by electron-phonon energy exchanges which increase the tip temperature until the vapor pressure of the Ga is sufficiently high to form a plasma that vaporizes a small portion of the emitter and causes a large electron pulse to propagate across the diode. Next the tip of the liquid cone reforms and the process repeats.

The energy exchange processes attending field emission, which have been studied previously,[34] cause the temperature of the tip T_o relative to the temperature T_1 at the base of the cone to vary according to

$$T_o - T_1 = \frac{kT \cot \pi p}{K} \left(\frac{I}{\alpha r}\right) + \frac{\rho(t)}{2K\pi^2} \left(\frac{I}{\alpha r}\right)^2 \qquad (37)$$

where K is the thermal conductivity, $\rho(t)$ is the electrical resistivity, r is the radius of the cone at the point of truncation and p is a dimensionless parameter given by

$$p = \frac{kT}{\alpha} \qquad (38)$$

The first term in Eq.(37) is due to so-called "Nottingham heating" and the second term is due to resistive heating.[34] It can be seen that for a

given value of $T_o - T$ the emission current I increases with cone half angle α. Arbitrarily taking a T_o value for a vapor pressure of 10^{-4} torr, a value of $I/\alpha r = 1.1 \times 10^4$ A/cm-rad is obtained for Ga. Thus, if $\alpha = 49°$ and $r = 500$ Å a value of $I \cong 50$ mA is obtained. Since Eq.(37) is derived for a steady state condition it is not likely to apply to our case where the pulse width is $< 10^{-8}$ sec. This means even higher currents may be obtainable during short pulses, which is in fact true.

In contrast, the ion emission mode exhibits a stable dc mode of operation. Apparently, under certain conditions, the cone apex radius is prevented from becoming infinitely small by the simultaneous removal of material by field evaporation. This leads to a steady state condition whereby the cone maintains itself at a constant apex radius by supplying material to the emitter apex at a rate equal to removal by field evaporation.

Future study will be directed at determining the optimum source configuration for long life operation and the angular and energy distribution of the emitted ions and electrons.

REFERENCES

1. J. R. Oppenheimer, Phys. Rev. 31, 67 (1928).
2. R. H. Fowler and L. W. Nordheim, Proc. Roy. Soc. A119, 173 (1928).
3. E. W. Müller, Z. Physik 106, 541 (1937); Z. Physik 131, 136 (1951).
4. D. B. Langmuir, Proc. Inst. Radio Eng. 25, 977 (1937).
5. J. Worster, J. Phys. D 2, 457 (1969).
6. J. Worster, J. Phys. D 2, 889 (1969).
7. L. W. Swanson and A. E. Bell, Adv. Elect. and Electr. Phys. 32, 193 (1973).
8. L. H. Veneklasen, Optik 36, 410 (1972).
9. I. C. Wiesner and T. E. Everhart, J. Appl. Phys. 44, 2140 (1973).
10. W. P. Dyke, J. K. Trolan, W. W. Dolan, G. Barnes, J. Appl. Phys. 24, 570 (1953).
11. J. Orloff and L. W. Swanson, J. Vac. Sci. Technol. 12, 1209 (1975).
12. L. W. Swanson and L. C. Crouser, J. Appl. Physics 40, 4741 (1969); L. W. Swanson, J. Vac. Sci. and Technol. 12, 1228 (1975).
13. L. W. Swanson and N. A. Martin, J. Appl. Phys. 46, 2029 (1975).
14. J. E. Wolfe, G. E. Ledges, H. H. Glascock, U.S. Patent 3,814,975 (1974).
15. M. I. Elinson and G. A. Kundintsevo, Rad. Eng. Elect. Phys. 7, 1417 (1962).
16. E. E. Windsor, Proc. IEE 116, 348 (1969).
17. L. W. Swanson, J. T. Dickinson and D. R. McNeely, NASA Contractor Report No. CR-2668 (1976).
18. P. Lebeau and J. Eiguras, Compt. Rend. 127, 393 (1898)
19. T. Aito, U. Kawabe, and Y. Honda, Japan J. Appl. Phys. 13, 391 (1974).
20. B. Post, D. Moskowitz, and F. W. Glaser, J. Am. Chem. Soc. 78, 1800 (1956).

References (Cont.)

21. J. P. Barbour, F. M. Charbonnier, W. W. Dolan, W. P. Dyke, E. E. Martin and J. K. Trolan, Phys. Rev. 117, 1452 (1960).

22. R. H. Good and E. W. Müller, Handbuch der Physik, 21, 176 (1956).

23. J. Waclawski and E. W. Müller, J. Appl. Phys. 32, 1472 (1961).

24. E. W. Müller and T. T. Tsong, Field Ion Microscopy, Principles and Applications (Elsevier, New York, 1969).

25. A. J. Jason, Phys. Rev. 156, 266 (1967).

26. I. W. Drummond and J. V. Long, The Production of Fine Ion Beams, Proc. 1st Int. Conf. on Ion Sources, Saclay (1969).

27. V. E. Krohn, Progr. Astron. Rocketry 5, 73 (1961).

28. E. Cohen, Rept. ARL-63-88, Space Technology Laboratories, Redondo Beach, Calif. (1963).

29. J. F. Mahoney, A. Y. Yahiku, H. L. Daley, R. D. Moore and J. Perel, J. Appl. Phys. 40, 5101 (1969).

30. D. S. Swatik and C. D. Hendricks, AIAA J. 6, 1596 (1968).

31. C. A. Evans, Jr. and C. D. Hendricks, Rev. Sci. Instr. 43, 1527 (1972).

32. B. N. Colby and C. A. Evans, Jr., Anal. Chem. 45, 1887 (1973).

33. G. Taylor, Proc. Roy. Soc. (London) A280, 383 (1964).

34. L. W. Swanson, L. C. Crouser and F. M. Charbonnier, Phys. Rev. 151, 327 (1966).